Analysis of neural circuits in vitro

by

Jennifer Lynn Wang

B.S., Physics, University of California, San Diego (2001)
B.A., Mathematics, University of California, San Diego (2001)

Submitted to the Department of Brain & Cognitive Sciences
in partial fulfillment of the requirements for the degree of

Doctor of Philosophy in Neuroscience

at the

MASSACHUSETTS INSTITUTE OF TECHNOLOGY

June 2010

Author .....
Department of Brain & Cognitive Sciences
May 12, 2010

Certified by .....
H. Sebastian Seung
Professor of Computational Neuroscience
Thesis Supervisor

Accepted by .....
Earl K. Miller
Picower Professor of Neuroscience
Chairman, Department Committee on Graduate Theses

Analysis of neural circuits in vitro

by

Jennifer Lynn Wang

Submitted to the Department of Brain & Cognitive Sciences
on May 12, 2010, in partial fulfillment of the
requirements for the degree of
Doctor of Philosophy in Neuroscience

Abstract

This thesis is a collection of manuscripts addressing connectivity of neural circuits in cultured hippocampal neurons. These studies begin with an investigation of dopaminergic modulation of excitatory synapses in small circuits of neurons grown on glial microislands. We found that dopamine transiently depressed excitatory synaptic transmission. Scaling up to larger circuits of neurons proved more challenging, since finding connected pairs became combinatorially more improbable. The discovery and use of light-activatable ion channel channelrhodopsin-2 (ChR2) promised to revolutionize the way in which we could map connectivity in vitro. We successfully delivered the gene for ChR2 in hippocampal cultures using recombinant adeno-associated virus and characterized the spatial resolution, as well as the reliability of stimulating action potentials. However, there were limitations to this technique that would render circuit maps ambiguous and incomplete. More recently, the engineering of rabies virus (RV) as a neural circuit tracer has produced an exciting method whereby viral infection can be targeted to a population of neurons and spread of the virus restricted to monosynaptically connected neurons. We further investigated potential mechanisms for previous observations which claim that RV spread is restricted to synaptically connected neurons by manipulating neural activity and synaptic vesicle release. We found that RV spread increased for blockade of synaptic vesicle exocytosis and for blockade of neural activity.

The underlying premise for pursuing these methods to elucidate connectivity is that the computational power of the brain comes from changeable, malleable connectivity and that to test network models of computation in a biological brain, we must map the connectivity between individual neurons. This thesis builds a framework for experiments designed to bridge the gap between computational learning theories and networks of live neurons.

Thesis Supervisor: H. Sebastian Seung
Title: Professor of Computational Neuroscience

Contents

Acknowledgements

I would first like to thank my advisor, Sebastian Seung, for being my scientific mentor, friend, and an endless source of inspiration. I am honored to have been able to learn the ways of science from him.

I am grateful to my committee members, Mark Bear, Carlos Lois, and Hongkun Park for their guidance and insights into this thesis work.

For the dopamine work, Jung Choi heroically perfected the microisland culture protocol we received from Yuki Goda.

For the ChR2 project, Maz Hasan graciously sent us the wonderful ChR2 virus and provided infectious enthusiasm for the project. Jeannine Foley provided the culture, and Seungeun Oh supplied optics wisdom for the laser stimulation system.

For the RV project, Ian Wickersham was the mastermind behind the constructs; Heather Sullivan was the culture and virus making guru; Srinivas Turaga provided the convolutional network (blank slate version); John Kaufhold supplied the crash course in bandpass filtering images; Uygar Sumbul, Kannan UV, Ignacio Arganda, and Daniel Berger helped me look at my images in different ways and taught me all about image analysis.

Seung lab members, past and present, who have contributed in many ways to my scientific development: Russ Tedrake, Ben Pearre, Justin Werfel, Ila Fiete, Xiaohui Xie, Dezhe Jin, Mark Goldman, Uri Rokni, Yonatan Loewenstein, Artem Starovoytov, Alan Chen, Naveen

Agnihotri, Brett Mensch, Sen Song, Viren Jain, and Matt Greene. All have been an amazing source of ideas and discussion about science and life.

Many thanks and my eternal gratitude to my classmate, labmate, and officemate Neville Sanjana, whose generous heart saw me through all my rough moments and believed in me, both as a person and scientist.

I would also like to thank Amy Dunn, administrator extraordinaire, for processing the countless orders and doing all the work that so often goes unnoticed but is so vital to getting science done. Many thanks to Denise Heintze and Brandy Baker, graduate administrators of Brain and Cognitive Sciences, for being so friendly and helping to keep me from falling through the cracks.

I am indebted to my undergraduate advisor David Kleinfeld, who gave me my first opportunity to do neuroscience by allowing me to work in his lab. Mrs. Packer, my high school biology and anatomy and physiology teacher, encouraged me to pursue science, way back in high school. Going back even further, I would like to thank Auntie Linda for taking me a countless number of times to the Seattle Science Center to see what happens when marshmallows get dunked in liquid nitrogen.

I've been incredibly lucky to have the following amazing climbing partners and friends, who have provided support and encouragement over the years: Maria-Louisa Izamis, Jim Wahl, John Cox, Dave Custer, Susan Ruff, Rachel Chapman, Laura Althoff, Nupur Lala, Liz Yoder, Amy Sun, Pam Godde, Marieann Margossian, Brian Tran, Shahe Diermendjian, and Kristin McLachlan (bluish green female sheep!).

I am grateful to Ming Wu and Jung Choi whose treatments and friendship keep me balanced and sane.

Most importantly, I would like to thank all of the Wangs, Chengs, and Lockes who have supported me all these years. I am especially grateful to my husband and best friend Simon Peffers, who went without dinner for a month while I finished this thesis and to Sebastian Peffers, whose 3 year old brain continues to fascinate me. Most of all, I thank my parents, Evelyn and William Wang, who believed in me all these years and encouraged and supported me with all their love, and my dear little brother Paul Wang, who makes me think about the brain all the time.

Chapter 1

Introduction

The following collection of papers comprising this thesis represents a progression of thought and technique addressing the study of monosynaptic connections in circuits of cultured hippocampal neurons. The major contributions of this thesis are as follows:

- Application of dopamine transiently depresses excitatory synapses in cultured hippocampal neurons grown on glial microislands
  - Developed microisland cultures which had small numbers of neurons isolated on glial islands. This increased the probability that neurons were connected to each other, and for isolated pairs of neurons, ruled out effects due to polysynaptic interaction.
  - Used the patch clamp technique to record simultaneously from monosynaptically connected pairs of neurons. Excitatory synapses were identified by reversal potential.
  - Bath application of dopamine transiently depressed excitatory synapses.
- Investigation of the spatial resolution and reliability of laser stimulation of neurons expressing ChR2 and assessment of ChR2 stimulation to map connectivity of neurons in culture
  - Delivered ChR2 gene to cultured hippocampal neurons using rAAV.
  - Optical stimulation of action potentials was more reliable in neurons older than DIV14.
  - A 40 μm diameter laser spot stimulated a larger fraction of neurons to reliably fire action potentials than a 10 μm diameter spot.
  - Scanned laser spot over culture to stimulate potential presynaptic partners of a patch clamped neuron.
  - Proposed criteria distinguishing between monosynaptic and polysynaptic responses recorded in a neuron postsynaptic to an optically-stimulated, ChR2-expressing presynaptic neuron.

- Blockade of activity and synaptic vesicle release increased RV spread in hippocampal culture
  - Validated the use of monosynaptically restricted RV in culture
  - Developed an image analysis pipeline to automate analysis of large numbers of images to assess the effects of drug manipulations on RV spread
  - Blocking synaptic vesicle release with botulinum toxin - A and tetanus toxin and blocking neural activity with action potential blocker TTX and synaptic blockers APV, CNQX, and bicuculline resulted in increased spread of RV. Application of partial block of dynamin-mediated endocytosis with dynasore resulted in a slight decrease of RV spread.

The study of neural circuits is the product of convergence in thought between the anatomical studies of Ramon y Cajal [18] and the electrophysiological studies of Hubel and Weisel [6]. There are many types of neurons in the brain, and how their connectivity could give rise to the many functional properties neuroscientists have observed is both an inscrutable and compelling problem [4]. That synapses are the intermediary unit between these two descriptions, places a large emphasis on understanding them, in particular, the modifications by which synapses increase or decrease in strength. This importance is underscored by the sheer immensity of literature on the experimental observations of synaptic modification and the structures and mechanisms involved[7].

The experiments presented here were motivated by the fact that reward is a powerful reinforcer of behavior [8] and the subsequent finding that activity of dopamine neurons signaled reward [10]. Given the observation that stimulation of the ventral tegmental area modulated cortical maps [1] and that dopamine could induce, as well as modulate certain forms of LTP [5, 9], there was the possibility that dopamine could effect these changes by synapses being the reward seeking agents themselves [11]. The hypothesis was that synaptic release, followed by reward would result in an increased probability of release. Conversely, rewarding synaptic failure would decrease the probability of release. Experimentally, this was a difficult question to address, requiring measurements from neurons with small, stochastic synapses. Because this was a hypothesis about vesicle release and failure, synaptically connected pairs of neurons were required.

We chose to pursue this hypothesis using cultures of hippocampal neurons. The use of culture to study connectivity is controversial because the endogenous 3 dimensional structure of the hippocampus is completely dissolved and networks regrown in a 2-dimensional sheet. Arguably, it is unnatural and questionable whether the resulting connectivity has any relationship to that of an intact brain. On the other hand, major phenomena observed in culture, such as LTP and homeostatic plasticity, have also been observed in brain slice and in vivo[2, 14], justifying the use of culture as a model system for investigating synapses. The benefits to using culture are that it provides easy access for imaging, electrophysiological recording, and genetic and pharmacological manipulation [13]. Our goal was not to claim that the connectivity we observed in culture was a stand-in for an intact brain. Instead, the goal was to verify a computational principle governing connectivity which might have analogue in intact brain.

In chapter 2, we engineered connectivity in hippocampal culture by restricting growth of neurons to glial microislands. Plating neurons at a low density on these microislands resulted in circuits of neurons that had small numbers of neurons. Recording from islands which contained only 2 synaptically connected neurons ensured that we were recording from a monosynaptically connected pair, connections uncontaminated by polysynaptic input. From those pairs we tested the effect of dopamine on excitatory synapses and found that dopamine transiently depressed these synapses.

While this system held great promise for pursuing the hedonistic synapse hypothesis, we found that microisland cultures were difficult to maintain, and the large synapses that were characteristic of two neuron islands were not ideal for experiments which required small, stochastic synapses. Using mass cultures provided a viable alternative. We found that synapses in mass cultures were smaller than those in the microisland cultures, but finding connected pairs of neurons was difficult. From pilot experiments, we observed a large range of synaptic changes in response to contigent application of dopamine, resulting in the need for many experiments to ensure reproducibility.

The search for a high-throughput method to identify small synapses begins in Chapter 3. The report of successful transfection of neurons with ChR2 and the subsequent demonstration that action potentials could be optically stimulated in these neurons with high temporal precision [3] provided a promising way to screen for connected neurons in mass cultures. We delivered the gene for ChR2 using recombinant adeno-associated virus and characterized the reliability and spatial resolution of laser stimulation for producing action potentials in neurons expressing ChR2. However, finding a criterion distinguishing between mono- and poly-synaptic responses in a patch clamped postsynaptic neuron was elusive. Additionally, there was a tradeoff between transfecting many neurons and preserving the spatial resolution of the optical stimulation. The more densely packed ChR2 expressing neurons were, the less likely sufficient optical stimulation would be guaranteed to stimulate only the targeted neuron. Expressing ChR2 in fewer neurons meant having fewer potential presynaptic targets to probe.

The engineering of monosynaptically restricted RV [17] appeared to be the ideal method for elucidating connectivity in culture. By defining a population of host neurons and limiting viral spread to neurons which were one synapse away, we could map all of the connections onto a given neuron. Chapter 4 explores the use of monosynaptically restricted RV in culture, as well as the activity dependence of viral spread to putatively connected neurons. The claim that RV spread is restricted to synaptically connected neurons comes from evidence that systems with known connectivity can be traced with high precision using RV. Additionally, the lack of local spread outside these well-defined systems is a strong indication of synaptic restriction [15, 12, 16]. Since synaptic transmission is a major determinant of connectivity, we hypothesized that synaptic vesicle release should be required for the virus to spread. Alternatively, neural activity might also be required. We investigated the effects of activity blockade and synaptic transmission blockade on spread of RV and found that both manipulations increased viral spread.

In closing, the hedonistic synapse hypothesis remains untested, but the framework and methodology for finding monosynaptically connected pairs of neurons in hippocampal culture might be of use to researchers interested in probing such connections. With the notion of cell type coming to the forefront of neural circuit analyses, there may be interest in inves-

tigating activity dependent plasticity mechanisms for different cell types. Additionally, the interplay between activity dependent plasticity and homeostatic plasticity could be further explored at the level of monosynaptically connected neurons. Recording from monosynaptically connected pairs is a laborious task, and we hope that our contributions toward making it more of a high-throughput endeavor will make it possible to try many more experimental conditions, obtain larger samples and thus higher reproducibility of findings to enhance our understanding of connectivity in the brain.

Chapter 2

Dopamine Transiently Depresses Excitatory Postsynaptic Currents in Cultured Rat Hippocampal Neurons

The following is a submitted manuscript.

Dopamine Transiently Depresses Excitatory Postsynaptic Currents in Cultured Rat Hippocampal Neurons

Jennifer Wang[1,*], Jung H. Choi[2], H. Sebastian Seung[3]

1 Department of Brain and Cognitive Sciences, Massachusetts Institute of Technology, Cambridge, MA, USA

2 Department of Brain and Cognitive Sciences, Massachusetts Institute of Technology, Cambridge, MA, USA

3 Department of Brain and Cognitive Sciences, Department of Physics, Massachusetts Institute of Technology, Howard Hughes Medical Institute, Cambridge, MA, USA

*** E-mail: jenwang@mit.edu**

Abstract

Background: Dopamine is a leading candidate for a reward signal in the brain and has also been implicated in many brain disorders. For these reasons, researchers have been interested in characterizing the effect of dopamine on synaptic transmission and plasticity. The reported effects of dopamine in the hippocampus have been diverse: different effects have been reported for different methodologies employed.

Methodology/Principal Findings: We have investigated the modulatory effects of dopamine on excitatory synaptic transmission using dual perforated patch clamp recordings of dissociated hippocampal neurons cultured from neonatal rats. Groups of a few neurons isolated on glial microislands were used for our experiments. Immunostaining revealed both D_1/D_5 and D_2 subtypes of the dopamine receptor in our cultured neurons. Bath application of 10 μM dopamine (DA) caused a rapid depression of excitatory postsynaptic currents. The effect was transient, in that synaptic currents recovered to baseline during a 15 minute washout period. While the D_1 agonist SKF 38393 produced a weaker transient depression that was on the edge of statistical significance, it did not fully replicate the effect of dopamine. The D_2 agonist quinpirole did not produce a significantly different result from control, nor did the combination of D_1 and D_2 agonists.

Conclusions/Significance: Our results are similar to previous reports of immediate and transient depression in brain slices of hippocampal CA1, as well as neocortical areas of the hippocampal formation.

Introduction

Dopamine has become a leading candidate for a reward signal in the brain [1,2], and plays an important role in current theories of reinforcement learning [3]. Dopamine has also been implicated in a number of brain disorders, such as Parkinson's disease [4, 5], schizophrenia [6], and ADHD [7]. For these reasons, researchers have been interested in characterizing the effects of dopamine on basic properties of neurons, such as intrinsic excitability [8–10] and synaptic transmission.

Electrophysiological studies have found that dopamine and its agonists have diverse effects on glutamatergic synaptic transmission. The effects depend on concentration, glutamate receptor subtype, dopamine receptor subtype, and brain region studied, which makes comparing results in the literature a confusing task. For brain slices of hippocampal CA1, researchers disagree over whether the effects of dopamine and its agonists are transient or persistent. Some find that synaptic transmission changes immediately upon bath application, and recovers to baseline within 10-15 minutes after washout. Others report that changes begin up to tens of minutes after bath application starts, and persist for up to hours after washout. As a rule, persistent changes have delayed onset, while transient changes develop rapidly (though one exception is noted below [11]). Those finding persistent changes do not report transient changes, and vice versa.

We now review the studies finding transient changes in more detail. Using intracellular recordings, Hsu showed that dopamine transiently depressed synaptic responses to Schaffer collateral stimulation [12]. Agonist and antagonist experiments suggested that this effect was mediated by the D_2 receptor. Using field potential recordings, Otmakhova and Lisman found that dopamine had little effect on synaptic responses to Schaffer collateral stimulation, except that the NMDA component was slightly depressed [13]. Instead, they found that dopamine transiently depresses synaptic responses to stimulation of the perforant path, including both the AMPA and NMDA components. Antagonist experiments suggested that both D_1 and D_2 receptors were involved.

In contrast to these findings of transient depression, Huang and Kandel found that D_1/D_5 agonists induce persistent potentiation of field potential responses to Schaffer collateral stimulation [14]. Later on, Yang confirmed this result using intracellular recording via whole cell patch clamp [15], but Mockett et al. could not replicate it using field potential recordings [16]. Using whole cell patch clamp recording, Varela et al. found that a D_1/D_5 agonist could produce either persistent potentiation or depression [11].

They found evidence that the sign of the effect depended on whether the NMDA receptors included NR2B subunits (potentiation) or NR2A subunits (depression). Since the NR2B subunit is predominant in the Schaffer collateral pathway, the Varela et al. result is consistent with the Huang and Kandel report of persistent potentiation. Since the NR2A subunit is predominant in the perforant pathway, the Varela et al. result is partially consistent with the Otmakhova and Lisman report of transient depression, except that their depression appears to be persistent and rapidly developing [13].

Finally, it should be mentioned that there is a subclass of the persistent studies in which dopamine is regarded as a modulator of long-term potentiation, defined as persistent potentiation induced by tetanic stimulation. Activation of D_1/D_5 receptors enhances the amplitude of early LTP [17], or is required for the maintenance of late LTP [18]. According to these studies, dopamine by itself is not sufficient to induce persistent potentiation; tetanic stimulation is required.

The diversity of these results may not be surprising, in light of the complexity of molecular mechanisms by which dopamine can affect glutamate receptors. Dopamine receptor activation can exert indirect effects through the second messenger cAMP [19]. Another mechanism is direct, involving protein-protein interactions between dopamine receptors and glutamate receptors [20]. Further complicating the picture is the fact that dopamine can also directly block the NMDA receptor pore without mediation by dopamine receptors [21–23].

Given the inconsistencies between physiological studies in the literature, we thought it worth using a different method to reexamine the effects of dopamine on synaptic transmission in hippocampal neurons. We applied the perforated patch clamp technique to record from pairs of hippocampal neurons cultured on glial microislands. Dissociated cultures can be criticized as more unnatural than acute brain slices, but our preparation also has a number of advantages. By recording from monosynaptically connected pairs of neurons, we avoid potential confounds due to polysynaptic pathways in the brain slice preparation. Compared to whole cell patch clamp, perforated patch clamp may have less adverse effects on intracellular signaling pathways. The brain slice preparation contains endogenous stores of dopamine that can be released by electrical stimulation [24], while our cultures presumably do not. Finally, wash-in and wash-out of dopamine is presumably faster in our cultures than in brain slices.

We have found that bath application of dopamine causes a transient depression of excitatory transmission, with no sign of persistent effects. Furthermore, the D_1 agonist SKF 38393 caused a weaker transient depression on the borderline of statistical significance. The D_2 agonist quinpirole, and a combination of

D_1 and D_2 agonists produced no statistically significant changes. We suggest that D_1 receptors could mediate the transient depression produced by dopamine, with the caveat that the effect of D_1 agonist was significantly different from that of dopamine. Our results are similar to those of Otmakhova and Lisman for perforant path synapses [13], although it is unclear whether the synapses in our cultured hippocampal neurons are homologous to those of the perforant path or Schaffer collaterals. Our work is also related to the recent experiments of Zhang et al., who like us used dual intracellular patch recordings of hippocampal neurons grown in dissociated cultures. They found that dopamine transiently depresses the NMDA receptor-mediated component of glutamatergic currents [25].

Materials and Methods

Microisland cultures

Ethics Statement

P1 Sprague-Dawley rat pups were used. All animal procedures were approved by the MIT Committee on Animal Care, in compliance with standards for the ethical use of laboratory animals set by the state of Massachusetts, the city of Cambridge, and the United States Animal Welfare Act.

P1 rat pups were anesthetized by chilling on ice, followed by decapitation. Hippocampi were extracted and solutions were prepared in a similar fashion to [26]. Hippocampi were collected with dentate gyrus removed and cut into small ($\approx$ 1 mm) pieces in a dissection solution containing 25 mM HEPES in Hank's Balanced Salt Solution (HBSS), pH 7.3. Some pieces were immediately dissociated for culture by incubating the tissue for 30-40 min at 37°C in HBSS containing 1 mM L-cysteine, 0.5 mM EDTA, 1.5 mM $CaCl_2$, 20 U/ml Papain (Worthington), and 0.1 μg/ml DNAase. The remaining pieces were stored for later use at 4°C in Hibernate E medium (Brain Bits), supplemented with 2% B27 (Invitrogen). The enzymatically dissociated tissue was rinsed 3 times in culture medium containing 6 mg/ml glucose, 1 mM Na-Pyruvate (Invitrogen), 10% fetal bovine serum (Hyclone), 0.1% Mito serum extender (Invitrogen), 2% B27 (Invitrogen), and 1 mM HEPES in Basal Medium Eagle (Invitrogen), pH 7.3 and then mechanically triturated with a fire polished plastic pipette in culture medium conditioned by incubating overnight at 37°C with a monolayer of glial cells in a culture flask.

To prepare glial microislands, cells were plated by adding 0.5 ml of cell suspension at 10,000 cells/ml

on glass coverslips coated with rat tail collagen in a 24-well plate. After 1 day in the incubator, 100 μl of 24 μM cytosine beta-D-arabinofuranoside (Ara-C) in culture medium was added to dampen proliferation. After 2 to 3 weeks, several microislands of glial cells were usually visible. The islands were generally 50-100 μm in diameter. If neurons remained on the islands, the cultures were kept outside the incubator at 4°C for a few hours to eliminate them.

Neurons were added to the glial islands 3-4 weeks later. These neurons were obtained by dissociating hippocampi that were either freshly dissected or stored for 3 days as described above. The cells were plated by aspirating culture medium from the well and adding 0.5 ml of cell suspension at 20,000 cells/ml on the glial microislands. A day or two later, 100 μl of culture medium was added (100μl of 24 μM Ara-C was added if needed to prevent glial proliferation). Neurons were used 8-14 days after plating on the glial microislands. We used microislands containing a few neurons, often just two.

Immunostaining

The cell culture was assayed for D_1/D_5 and D_2 dopamine receptor subtypes [27] using rabbit anti-human dopamine D_1 (1:100) and goat anti-human dopamine D_2 (1:50) primary antibodies (Santa Cruz Biotechnology, Inc.). The respective binding of these antibodies to their substrates was detected using secondary antibodies Alexa Fluor 488 donkey anti-rabbit IgG (1:400) and Alexa Fluor 546 donkey anti-goat IgG (1:400) (Molecular Probes).

The cells were fixed in formalin for 20 min at room temperature, rinsed 3 times with phosphate buffered saline (PBS), and permeabilized in 0.25% Triton in PBS for 10 min at room temperature. Random binding of the primary was blocked with 4% donkey serum in PBS. The cells were then incubated at 37°C for 1 hr with both primary antibodies. They were rinsed 3 times with PBS, incubated at 37°C for 45 min with the secondary antibodies, and rinsed 3 more times with PBS. To control for random binding of the secondary antibodies, cells were fixed and permeabilized as above, and then incubated with the secondary antibodies only.

The cells were visualized with an inverted, phase contrast microscope (Olympus IX70). Excitation and emission of the secondary antibodies was produced using FITC and TRITC cubes (Chroma) with a mercury arc lamp source. Images were acquired using a Sensicam QE high speed CCD camera (Cooke), controlled by CamWare (Cooke) software.

Electrophysiology

Dual whole-cell perforated patch recordings were performed using the Multiclamp 700A patch clamp amplifier (Axon Instruments). Signals were filtered at 6 kHz and sampled at 10 kHz using a PCI-6052E A/D board (National Instruments). Micropipettes were pulled from glass capillaries (Warner) and had a 2-3 MΩ resistance. The pipettes were back-filled with an internal solution containing 300 μg/ml amphotericin B (Sigma) in 1% DMSO for membrane perforation. The internal solution of the pipette contained (in mM) potassium gluconate 136.5, KCl 17.5, NaCl 9, $MgCl_2$ 2, pH 7.30. [28] We determined that perforation had occurred when the access resistance stabilized and was no longer decreasing. This generally happened when the access resistance was between 20 MΩ and 40 MΩ with fluctuations less than 15%. The neurons were bathed in a HEPES-buffered saline (HBS) containing (in mM) NaCl 145, KCl 3, HEPES 10, $CaCl_2$ 3, glucose 8, $MgCl_2$, pH 7.30. [28] Recordings were done at room temperature.

To determine synaptic connectivity, the postsynaptic cell was stepped in voltage clamp, from −70 to −10 mV in 10 mV increments, while the presynaptic cell was stimulated in voltage clamp to fire an action potential in voltage clamp with a +120 mV pulse applied for 1.5 msec. In this way, the synaptic reversal potential could be determined. Typically, IPSCs reversed between −50 and −30 mV and had a ~100 ms time constant, while EPSCs (glutamatergic currents) showed no reversal for the given voltage steps and had a shorter time constant of ~10 ms. The use of reversal potential to determine transmitter type was verified for a few examples by blocking glutamatergic currents with 10 μM CNQX and 100 μM APV (Sigma). In the representative example shown in Figure 1A, the estimated reversal potential was greater than −10 mV, so we classified the synaptic current as an EPSC. Application of CNQX was sufficient to block synaptic transmission (Figure 1B), confirming glutamatergic transmission. Conversely, in Figure 1C, the estimated reversal potential was −40 mV, so we classified the synaptic current as an IPSC. Application of CNQX and APV did not alter synaptic transmission (Figure 1D), which showed that IPSCs were not mediated by glutamatergic transmission. We did not use synaptic blockers for all experiments; we measured the reversal potential instead, since it seemed a reliable indicator of transmitter type. For our experiments, we used pairs which had reversal potential greater than −10 mV.

To measure evoked EPSCs, the presynaptic cell was stimulated in voltage clamp by stepping from −70 mV to 50 mV for 1 ms once every 30 sec while holding the postsynaptic cell at −70 mV. The PSC amplitude was measured from a smoothed (0.5 ms boxcar) version of the current trace by taking the difference between the current just before onset of the PSC and the trough. PSC amplitudes ranged from

50-700 pA and had simple shapes, indicating monosynaptic responses. Pairs selected for analysis had access resistance between 15 and 40 MΩ and leak current less than −150 pA. Additionally, recordings in which postsynaptic currents exhibited correlated changes with access resistance were discarded. Custom software written in Matlab was used to perform the experiments and analyze the data.

Dopamine and agonists

The dopamine (DA) solution was prepared immediately before bath application, as dopamine is known to degrade rapidly through oxidation. If the solution was not freshly made, the effects reported in this paper became weaker (data not shown). We avoided using ascorbic acid as an anti-oxidant, because of its effects on neural excitability [29].

The D_1 agonist R(+)SKF-38393 (Sigma) and D_2 agonist (-)Quinpirole (Sigma) were kept at −20°C as 10 mM stock solutions in Millipore filtered water. They were diluted to 10 μM in HBS immediately before bath application.

Bath application of drugs

All experiments consisted of three periods: (1) a baseline lasting 5 minutes, (2) drug application for 5 minutes, and (3) washout for 15 minutes. The bath solution was continually renewed using a peristaltic pump (Rainin) at a base flow rate of 40 ml/hr. At the beginning of the drug application period, the intake of the peristaltic pump was exchanged to bath solution containing the drug. The flow rate was increased to maximum for 30 seconds to rapidly exchange the new solution. For the rest of the drug application period, the flow rate was returned to the base value of 40 ml/hr. At the beginning of the washout period, the intake of the peristaltic pump was exchanged to bath solution with no drug, and a similar procedure was followed.

In control experiments, the flow rate of the peristaltic pump was manipulated with the same time course, but with no change of solutions.

Results

Using the procedures described in the Methods, we produced cultures containing glial microislands and hippocampal neurons at very low density (see Figure $2A_1$ for representative phase contrast image). *In*

vivo, the hippocampus receives dopaminergic innervation from the ventral tegmental area (VTA) [30] and contains dopamine receptors [31, 32]. Since our cultures presumably did not contain dopaminergic neurons, it was unclear whether the hippocampal neurons would continue to express dopamine receptors. This was checked by double immunostaining for D_1 and D_2 receptors, which revealed that expression is present *in vitro* (Figure 2B and C).

Synaptic transmission between pairs of neurons was measured using dual patch clamp recordings (Figure 3A). For each recording, we located a glial microisland containing two to four neurons, and voltage clamped two of them. The presynaptic neuron was stimulated to produce an action potential while the postsynaptic neuron was recorded to measure synaptic transmission. If synaptic currents were observed, the reversal potential was found by varying the voltage of the postsynaptic neuron (see Methods). If the reversal potential was consistent with glutamatergic transmission, then an experiment was performed.

Every experiment used the same protocol. After the access resistance of the recording stabilized (see Methods), the presynaptic neuron was stimulated to generate a single action potential once every 30 seconds. The postsynaptic current was measured during three periods: (1) baseline for 10 minutes (2) drug application for 5 minutes (3) washout for 15 minutes. For each recorded pair of neurons, the time series of EPSC amplitudes was normalized by dividing by the average EPSC amplitude during the baseline period. The normalized time series were averaged over neuron pairs to produce the graphs in Figure 3. Three drugs were each applied singly: dopamine (DA), the D_1 agonist SKF 38393, and the D_2 agonist quinpirole. In a fourth manipulation, both D_1 and D_2 agonists were applied in combination. All drugs were used at 10 μM concentrations.

Figure 3B shows the average time course of EPSC amplitude during the DA experiments. The amplitude depresses immediately after the start of bath application of DA. By the end of the 5 minute DA period, the EPSC amplitude is less than 40% of its baseline value. During the 15 minute washout period, the EPSC recovers steadily. Shown for comparison is the average time series from control experiments with no drug.

In Figure 3C, application of D_1 agonist causes depression of the EPSC amplitude. The effect is strongest at the end of the 5 minute period of agonist application. The average depression during the agonist application is not as strong as that observed with DA. In Figure 3D, application of D_2 agonist causes some depression of EPSC amplitude. This time the effect looks strongest near the beginning of

the 5 minute period of agonist application. Overall, the depression is even weaker than that observed with D_1 agonist.

It is not clear why DA produced a stronger depression than the agonists. We conjectured that DA produces a stronger effect by stimulating both D_1 and D_2 receptors. To test this hypothesis, we applied a combination of D_1 and D_2 agonists, but this produced little or no effect (Figure 3E).

To test for the significance of these effects, we performed two types of statistical analysis. The first type of analysis is based on the various averages shown in Figure 3. In Figure 4A, each experiment is summarized by a single number quantifying the amount of depression, calculated by averaging the normalized EPSC amplitude during the 5 minute bath application period.

To compare the five conditions of (1) dopamine ($n = 6$), (2) D1 agonist ($n = 8$), (3) D2 agonist ($n = 8$), (4) D1+D2 agonist ($n = 7$), and (5) control ($n = 5$), we performed an analysis of variance (ANOVA), followed by the Tukey-Kramer test to identify pairs of conditions that were statistically significant (MATLAB Statistics Toolbox). The ANOVA rejected the null hypothesis that all conditions are the same. By the Tukey-Kramer test, dopamine is significantly different from the other conditions 2-5, which include both the control and the agonists. Conditions 2-5 are not significantly different from each other.

As a second test of statistical significance, we did not time average the data during the bath application period. Figure 4B shows these data for the different drugs. In this analysis, an experiment is not represented by a single average number, but by several data points taken at times during the bath application period. These data points are assumed to be statistically independent measurements. This assumption would be true if the fluctuations were due only to measurement noise. However, there also appear to be correlated fluctuations; the data points from a single experiment might tend to be all above-average or all below-average. Therefore we apply the second test of statistical significance with the caveat that its results are probably not conservative enough. We considered only data points from the second half of the bath application period, because it can take some time for the effects of the drug to set in.

Again the ANOVA rejected the null hypothesis that all conditions are the same. By the Tukey-Kramer test, the dopamine and D1 agonist experiments are significantly different from each other, and from all other conditions. The other conditions (D2 agonist, D1+D2 agonist, and control) are not significantly different from each other.

Discussion

We have found that bath application of dopamine causes a rapidly developing depression of excitatory synaptic transmission in hippocampal neurons. During the 15 minute washout period, synaptic currents recover to their baseline values, so that the depression is transient. Our finding of an immediate and transient depression is similar to previous reports in brain slices of hippocampal CA1 [12, 13].

The D_1 agonist SKF 38393 also induced a weak transient depression. However, the effect was not significantly different from control by the Tukey-Kramer test based on the time averages of experiments. The effect was significant if the data points from an experiment were not averaged, but this statistical analysis cannot be completely trusted because the fluctuations at different times are likely to be correlated. We conclude that the effect of D_1 agonist is on the borderline of significance. However, by both types of statistical analysis, the effect of the D1 agonist is significantly different from that of dopamine. A weaker effect is consistent with the fact that SKF 38393 is regarded as a partial rather than full agonist of the D_1 receptor [33]. The D_2 agonist quinpirole caused an even weaker transient depression. The effect was not significant by either statistical analysis.

We suggest that D_1 receptors could mediate the effects of dopamine on synaptic transmission. This is similar to the conclusion that Otmakhova and Lisman reached for perforant path synapses using antagonist experiments [13]. It does not match Hsu's finding that transient depression in the Schaffer collateral pathway is mediated solely by D_2 receptors [12].

Finally, we found that a combination of the D_1 and D_2 agonists was not significantly different from control. In other words, the effect produced by the combination of agonists was less than the effect produced by the D_1 agonist. We speculate that this is related to the fact that the D_1 and D_2 receptors have antagonistic effects on levels of the second messenger cAMP, as well as on phosphorylation of DARPP-32 [19].

Based on the results with agonists, we cannot completely exclude the possibility that dopamine is acting directly on the NMDA receptor pore, rather than indirectly through dopamine receptors [21–23].

Recently Zhang et al. published another study about the effects of dopamine on long-term plasticity of glutamatergic synapses between hippocampal neurons grown in dissociated cultures [25]. As an aside, they also mentioned that dopamine transient depresses synaptic transmission. They observed a significant effect when AMPA receptor currents were blocked. They also observed a weaker effect without synaptic

blockers, but the effect was not statistically significant. They did not report whether these effects could be replicated with dopamine agonists. To speculate about the slight differences between their results and ours, we note there are two differences in methods. They used ascorbic acid to retard the oxidation of dopamine in solution, and they cultured embryonic neurons rather than postnatal neurons.

In conclusion, we join the ranks of researchers who have reported transient depression of excitatory hippocampal synapses by dopamine [12, 13], as opposed to persistent potentiation [14, 15]. Transient depression is also a common finding in neocortical areas of the hippocampal formation. Behr et al. showed that dopamine and a D_1 agonist transiently depress excitatory synaptic currents in subicular neurons, while a D_2 agonist did not [34]. Pralong and Jones found that dopamine transiently depressed excitatory synaptic currents in entorhinal cortex neurons [35]. Based on antagonist experiments, they tentatively concluded that D_1 receptors were more likely to be involved. Similar results have also been reported in brain slices of prefrontal cortex [36], nucleus accumbens [37, 38], and basal forebrain [39].

Acknowledgments

References

1. Schultz W (1998) Predictive reward signal of dopamine neurons. J Neurophysiol 80: 1–27.

2. Schultz W (2002) Getting formal with dopamine and reward. Neuron 36: 241–263.

3. Montague P, Dayan P, Sejnowski T (1996) A framework for mesencephalic dopamine systems based on predictive hebbian learning. Journal of Neuroscience 16: 1936–1947.

4. Dauer W, Przedborski S (2003) Parkinson's disease mechanisms and models. Neuron 39: 889–909.

5. Olanow C, Tatton W (1999) Etiology and pathogenesis of parkinson's disease. Annual review of neuroscience 22: 123–144.

6. Davis K, Kahn R, Ko G, Davidson M (1991) Dopamine in schizophrenia: a review and reconceptualization. American Journal of Psychiatry 148: 1474–1486.

7. LaHoste GJ, Swanson JM, Wigal SB, Glabe C, Wigal T, et al. (1996) Dopamine d4 receptor gene polymorphism is associated with attention deficit hyperactivity disorder. Mol Psychiatry 1: 121–4.

8. Calabresi P, Mercuri NB, Sancesario G, Bernardi G (1993) Electrophysiology of dopamine-denervated striatal neurons. implications for parkinson's disease. Brain 116 (Pt 2): 433–52.

9. Centonze D, Gubellini P, Pisani A, Bernardi G, Calabresi P (2003) Dopamine, acetylcholine and nitric oxide systems interact to induce corticostriatal synaptic plasticity. Reviews in the neurosciences 14: 207–16.

10. Chen L, Bohanick JD, Nishihara M, Seamans JK, Yang CR (2007) Dopamine d1/5 receptor-mediated long-term potentiation of intrinsic excitability in rat prefrontal cortical neurons: Ca2+-dependent intracellular signaling. Journal of neurophysiology 97: 2448–64.

11. Varela J, Hirsch S, Chapman D, Leverich L (2009) D1/d5 modulation of synaptic nmda receptor currents. Journal of Neuroscience 29: 3109–3119.

12. Hsu K (1996) Characterization of dopamine receptors mediating inhibition of excitatory synaptic transmission in the rat hippocampal slice. J Neurophysiol 76: 1887–1895.

13. Otmakhova N, Lisman J (1999) Dopamine selectively inhibits the direct cortical pathway to the ca1 hippocampal region. J Neurosci 19: 1437–1445.

14. Huang Y, Kandel E (1995) D1/d5 receptor agonists induce a protein synthesis-dependent late potentiation in the ca1 region of the hippocampus. Proc Natl Acad Sci U S A 92: 2446–50.

15. Yang S (2000) Sustained enhancement of ampa receptor- and nmda receptor-mediated currents induced by dopamine d1/d5 receptor activation in the hippocampus: an essential role of postsynaptic ca2+. Hippocampus 10: 57–63.

16. Mockett B, Brooks W, Tate W, Abraham W (2004) Dopamine d1/d5 receptor activation fails to initiate an activity-independent late-phase ltp in rat hippocampus. Brain Res 1021: 92–100.

17. Otmakhova N, Lisman J (1996) D1/d5 dopamine receptor activation increases the magnitude of early long-term potentiation at ca1 hippocampal synapses. J Neurosci 16: 7478–86.

18. O'Carroll CM, Morris RGM (2004) Heterosynaptic co-activation of glutamatergic and dopaminergic afferents is required to induce persistent long-term potentiation. Neuropharmacology 47: 324–32.

19. Greengard P (2001) The neurobiology of slow synaptic transmission. Science 294: 1024–1030.

20. Lee FJS, Xue S, Pei L, Vukusic B, Chéry N, et al. (2002) Dual regulation of nmda receptor functions by direct protein-protein interactions with the dopamine d1 receptor. Cell 111: 219–30.

21. Castro NG, de Mello MC, de Mello FG, Aracava Y (1999) Direct inhibition of the n-methyl-d-aspartate receptor channel by dopamine and (+)-skf38393. Br J Pharmacol 126: 1847–55.

22. Masuko T, Suzuki I, Kizawa Y, Kusama-Eguchi K, Watanabe K, et al. (2004) Monoamines directly inhibit n-methyl-d-aspartate receptors expressed in xenopus oocytes in a voltage-dependent manner. Neurosci Lett 371: 30–3.

23. Cui C, Xu M, Atzori M (2006) Voltage-dependent block of n-methyl-d-aspartate receptors by dopamine d1 receptor ligands. Molecular Pharmacology 70: 1761–1770.

24. Frey U, Schroeder H, Matthies H (1990) Dopaminergic antagonists prevent long-term maintenance of posttetanic ltp in the ca1 region of rat hippocampal slices. Brain Res 522: 69–75.

25. Zhang JC, Lau PM, Bi GQ (2009) Gain in sensitivity and loss in temporal contrast of stdp by dopaminergic modulation at hippocampal synapses. Proc Natl Acad Sci USA 106: 13028–33.

26. Hagler J, Goda Y (2001) Properties of synchronous and asynchronous release during pulse train depression in cultured hippocampal neurons. J Neurophysiol 85: 2324–34.

27. Aizman O, Brismar H, Uhlén P, Zettergren E, Levey AI, et al. (2000) Anatomical and physiological evidence for d1 and d2 dopamine receptor colocalization in neostriatal neurons. Nat Neurosci 3: 226–30.

28. Bi G, Poo M (1998) Synaptic modifications in cultured hippocampal neurons: dependence on spike timing, synaptic strength, and postsynaptic cell type. J Neurosci 18: 10464–72.

29. Sutor B, Bruggencate GT (1990) Ascorbic acid: a useful reductant to avoid oxidation of catecholamines in electrophysiological experiments in vitro? Neurosci Lett 116: 287–92.

30. Gasbarri A, Verney C, Innocenzi R, Campana E, Pacitti C (1994) Mesolimbic dopaminergic neurons innervating the hippocampal formation in the rat: a combined retrograde tracing and immunohistochemical study. Brain Res 668: 71–9.

31. Huang Q, Zhou D, Chase K, Gusella J, Aronin N, et al. (1992) Immunohistochemical localization of the d1 dopamine receptor in rat brain reveals its axonal transport, pre- and postsynaptic localization, and prevalence in the basal ganglia, limbic system, and thalamic reticular nucleus. Proc Natl Acad Sci U S A 89: 11988–92.

32. Levey A, Hersch S, Rye D, Sunahara R, Niznik H, et al. (1993) Localization of d1 and d2 dopamine receptors in brain with subtype-specific antibodies. Proc Natl Acad Sci U S A 90: 8861–5.

33. Setler P, Sarau H, Zirkle C, Saunders H (1978) The central effects of a novel dopamine agonist. European journal of pharmacology 50: 419–430.

34. Behr J, Gloveli T, Schmitz D, Heinemann U (2000) Dopamine depresses excitatory synaptic transmission onto rat subicular neurons via presynaptic d1-like dopamine receptors. J Neurophysiol 84: 112–9.

35. Pralong E, Jones R (1993) Interactions of dopamine with glutamate- and gaba-mediated synaptic transmission in the rat entorhinal cortex in vitro. Eur J Neurosci 5: 760–7.

36. Gao W, Krimer L, Goldman-Rakic P (2001) Presynaptic regulation of recurrent excitation by d1 receptors in prefrontal circuits. Proc Natl Acad Sci U S A 98: 295–300.

37. Harvey J, Lacey M (1996) Endogenous and exogenous dopamine depress epscs in rat nucleus accumbens in vitro via d1 receptors activation. J Physiol 492 (Pt 1): 143–54.

38. Nicola S, Kombian S, Malenka R (1996) Psychostimulants depress excitatory synaptic transmission in the nucleus accumbens via presynaptic d1-like dopamine receptors. J Neurosci 16: 1591–604.

39. Momiyama T, Sim J, Brown D (1996) Dopamine d1-like receptor-mediated presynaptic inhibition of excitatory transmission onto rat magnocellular basal forebrain neurones. J Physiol 495 (Pt 1): 97–106.

Figure Legends

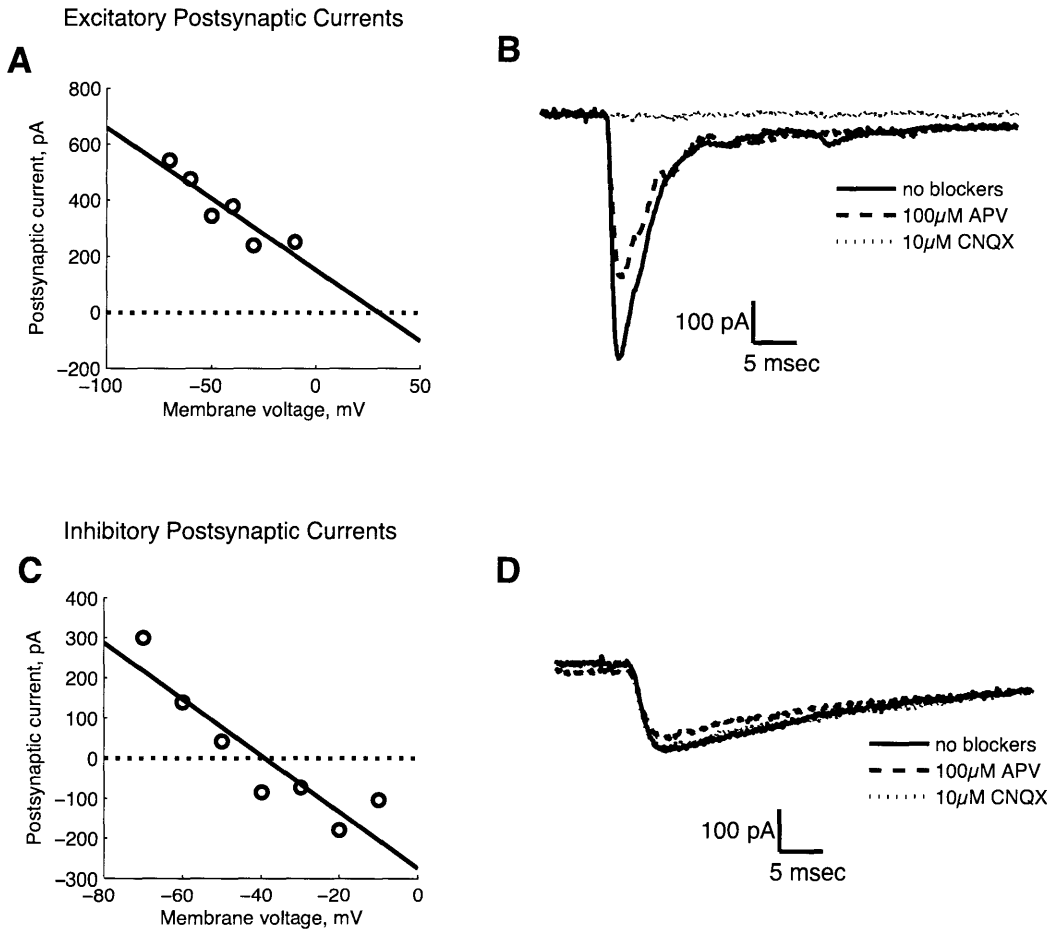

Figure 1. Validating reversal potential as a method to select glutamatergic synapses. In panels (A) and (C), we show current-voltage (I-V) plots for two synapses, which serve as representative examples. The open circles are EPSC amplitudes (y-axis) measured for varying postsynaptic holding potentials (x-axis). The solid line is a least squares fit to indicate the estimated reversal potential (intersection with dotted line). In (A), the estimated reversal potential is greater than -10 mV, so we classified the synaptic current as an EPSC. Panel (B) shows that application of 10 μM CNQX is sufficient to block transmission, confirming that excitatory synaptic transmission is glutamatergic. An example of an inhibitory synapse is shown in (C) and (D). The estimated reversal potential was -40 mV (C), so we classified the synaptic current as an IPSC. Neither CNQX or APV had an effect on synaptic transmission (D), consistent with the notion that IPSCs were not mediated by glutamatergic transmission.

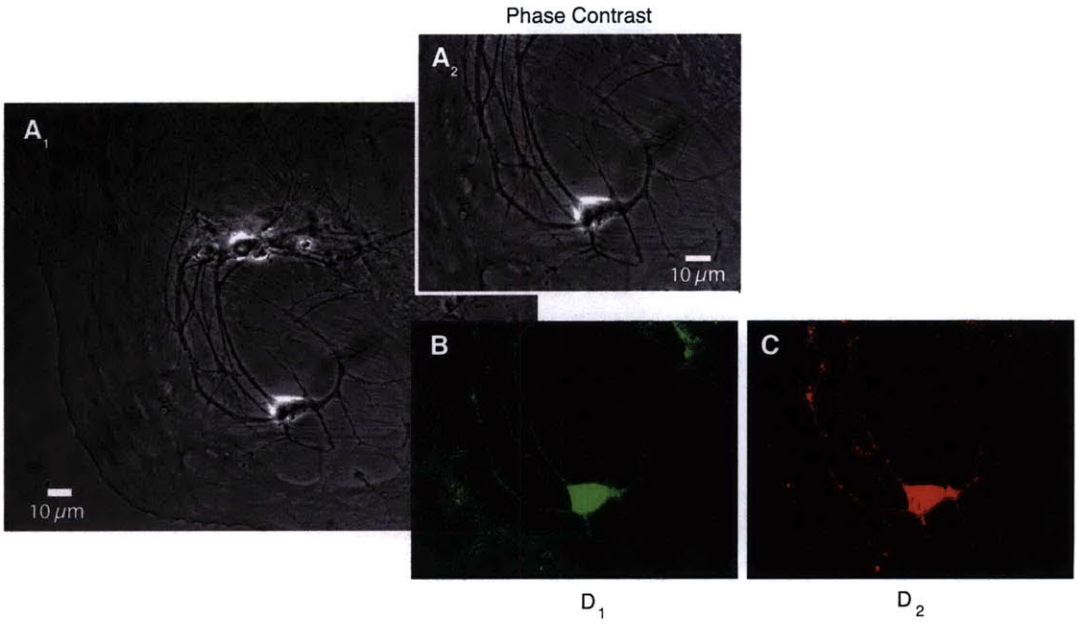

Figure 2. Hippocampal culture expresses D_1 and D_2 subtypes of the dopamine receptor. Phase contrast image at 40× magnification of culture grown on glial microisland (A_1). A magnified version is shown in A_2. Pseudocolored fluorescent images showing D_1 (1:100) expression (B) and D_2 (1:50) expression (C) using the same field of view as in A_2.

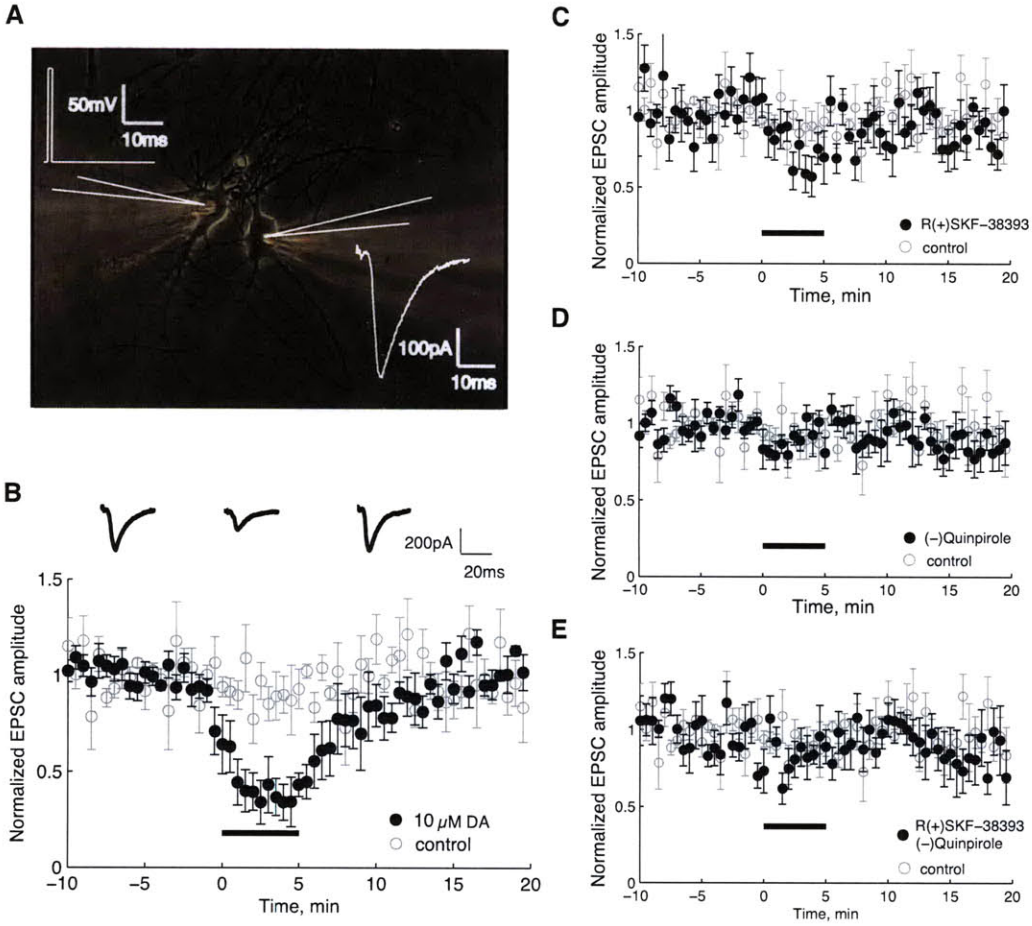

Figure 3. Bath application of dopamine and D_1, D_2 agonists results in a transient depression of EPSC amplitude. Bath application of dopamine and D_1/D_2 agonists results in a transient depression of EPSC amplitude. A schematic (white) of the dual patch clamp experiment is shown in (A), overlaid on a 40x phase contrast image of two neurons isolated on a glial island. The presynaptic neuron (left) was stimulated in voltage clamp to fire an action potential by stepping the membrane potential of the cell from -70 mV to 50 mV for 1 ms. An EPSC was recorded in the voltage clamped postsynaptic neuron (right). The time series of averaged, normalized EPSC amplitudes are shown in (B-E, closed black circles) for the 3 phases of the experiment - baseline, drug application, and washout. The control condition, where no drug was applied, is shown for comparison (open gray circles, $n = 5$). The error bars represent the standard error. In (B), we applied 10 μM DA during the bath perfusion period ($n = 6$). Above the time series are three representative EPSCs selected from the corresponding phase of the experiment. In (C), we applied 10 μM D_1 agonist R(+)SKF-38393 ($n = 8$) during the drug application period, and in (D), we applied 10 μM D_2 agonist (-)Quinpirole ($n = 8$). In (E), we applied a combination of 10 μM R(+)SKF-38393 and 10 μM (-)Quinpirole ($n = 7$).

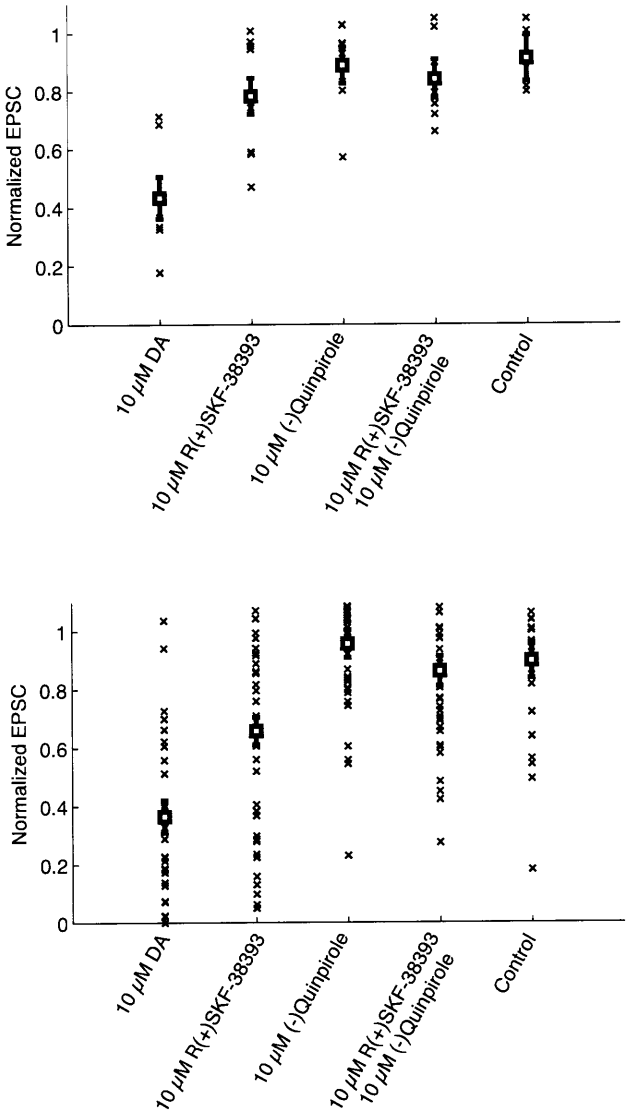

Figure 4. Summary of data from the bath application experiments. (A) Distribution of average normalized EPSC amplitude during the drug application period for each pair. Drug is indicated on the x-axis, and each point (x) represents a pair. The bold squares with error bars represent the ANOVA estimate for the mean and standard error, respectively, for each group. The DA condition was significantly different from control and all other conditions, using the Tukey-Kramer comparison test. (B) Distribution of EPSC amplitudes taken from the second half of the perfusion period. Each point (x) represents an individual, non-averaged value for EPSC amplitude. Drug is indicated on the x-axis. The ANOVA estimate for the mean and standard error are also shown (bold squares and error bars, respectively). The DA and D_1 conditions were significantly different from each other and all other conditions, including control, by the Tukey-Kramer comparison test.

Chapter 3

Laser-evoked synaptic transmission in cultured hippocampal neurons expressing channelrhodopsin-2 delivered by adeno-associated virus

The following paper has been published.

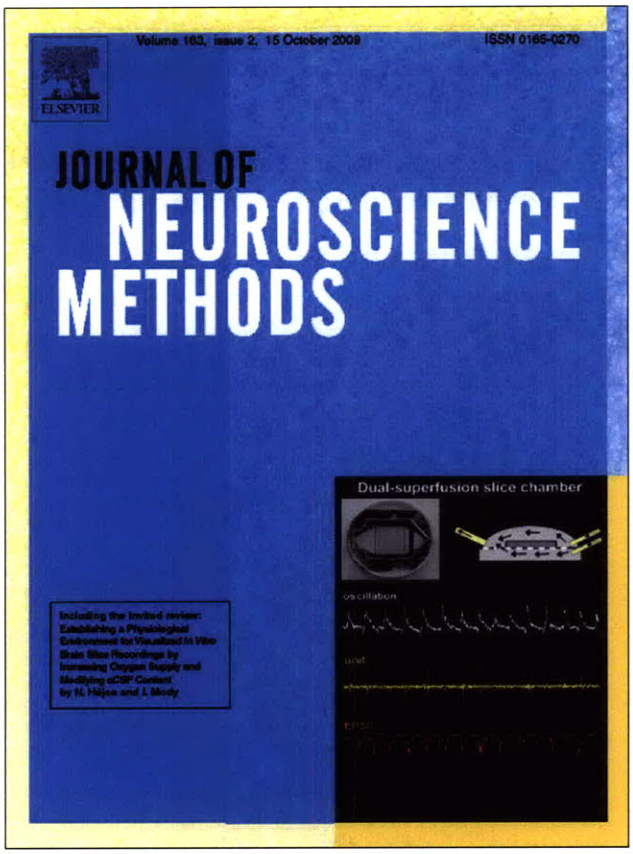

Journal of Neuroscience Methods 183 (2009) 165–175

Contents lists available at ScienceDirect

Journal of Neuroscience Methods

journal homepage: www.elsevier.com/locate/jneumeth

Laser-evoked synaptic transmission in cultured hippocampal neurons expressing channelrhodopsin-2 delivered by adeno-associated virus

Jennifer Wang[a,*], Mazahir T. Hasan[b], H. Sebastian Seung[c]

[a] Department of Brain and Cognitive Sciences, Massachusetts Institute of Technology, 77 Massachusetts Avenue 46-5065, Cambridge, MA 02139 United States
[b] Max Planck Institute for Medical Research, 29-Jahnstrasse, D-69120 Heidelberg, Germany
[c] Departments of Brain and Cognitive Sciences and Physics, Massachusetts Institute of Technology, Howard Hughes Medical Institute, 77 Massachusetts Avenue 46-5065, Cambridge, MA 02139, United States

ARTICLE INFO

Article history:
Received 1 April 2009
Received in revised form 17 June 2009
Accepted 18 June 2009

Keywords:
Channelrhodopsin-2 (ChR-2)
Recombinant adeno-associated virus (rAAV)
Synaptic physiology
Primary hippocampal culture

ABSTRACT

We present a method for studying synaptic transmission in mass cultures of dissociated hippocampal neurons based on patch clamp recording combined with laser stimulation of neurons expressing channelrhodopsin-2 (ChR2). Our goal was to use the high spatial resolution of laser illumination to come as close as possible to the ideal of identifying monosynaptically coupled pairs of neurons, which is conventionally done using microisland rather than mass cultures. Using recombinant adeno-associated virus (rAAV) to deliver the ChR2 gene, we focused on the time period between 14 and 20 days *in vitro*, during which expression levels are high, and spontaneous bursting activity has not yet started. Stimulation by wide-field illumination is sufficient to make the majority of ChR2-expressing neurons spike. Stimulation with a laser spot at least 10 μm in diameter also produces action potentials, but in a reduced fraction of neurons. We studied synaptic transmission by voltage-clamping a neuron with low expression of ChR2 and scanning a 40 μm laser spot at surrounding locations. Responses were observed to stimulation at a subset of locations in the culture, indicating spatial localization of stimulation. Pharmacological means were used to identify responses that were synaptic. Many responses were of smaller amplitude than those typically found in microisland cultures. We were unable to find an entirely reliable criterion for distinguishing between monosynaptic and polysynaptic responses. However, we propose that postsynaptic currents with small amplitudes, simple shapes, and latencies not much greater than 8 ms are reasonable candidates for monosynaptic interactions.

1. Introduction

The cloning of channelrhodopsin-2 (ChR2) and subsequent expression in mammalian cells promised to revolutionize neurophysiology because it enabled optical stimulation of neurons in a spatially localized and temporally precise fashion (Boyden et al., 2005; Nagel et al., 2003; Wang et al., 2007). ChR2 has been used to identify presynaptic partners of an electrophysiologically recorded postsynaptic neuron (Arenkiel et al., 2007; Petreanu et al., 2007; Wang et al., 2007). Other applications include mapping neuronal circuits, probing synaptic function in genetically defined populations of neurons, and inducing plasticity at single synapses (Atasoy et al., 2008; Liewald et al., 2008; Wang et al., 2007; Zhang et al., 2008; Zhang and Oertner, 2007). In principle, ChR2 could also be used to study the responses of networks to complex spatiotemporal patterns of stimulation.

Expression of ChR2 in neurons has been achieved by mouse transgenesis (Arenkiel et al., 2007; Wang et al., 2007); *in utero* electroporation (Petreanu et al., 2007), lentivirus (Boyden et al., 2005) and recombinant adeno-associated virus (rAAV) (Bi et al., 2006). A major drawback of lentivirus is that its DNA integrates into the host genome. Therefore the transgene is potentially susceptible to integration-induced epigenetic silencing (Ellis, 2005; Xia et al., 2007). Furthermore, a host gene could be disrupted by lentivirus DNA integration, which could affect normal neuronal function. Although mouse transgenesis by oocyte DNA injection is a powerful tool, integration of exogenous DNA at specific sites can lead to integration-induced gene silencing (Clark et al., 1997; Robertson et al., 1996) and position-effect variegation (Robertson et al., 1995) with gene expression in some cells but not others. Although a plasmid delivered by *in utero* electroporation remains extrachromasomal, which may alleviate the silencing problem, transfection of early progenitor cells leads to mosaic gene expression in neuronal populations of the postnatal brain (Borrell et al., 2005; Hatanaka et al., 2004).

Recombinant adeno-associated virus gene delivery has been successfully used to express ChR2 in mouse retinal neurons, and

* Corresponding author. Tel.: +1 617 452 2691; fax: +1 617 452 2913.
E-mail address: jenwang@mit.edu (J. Wang).

0165-0270/$ – see front matter © 2009 Elsevier B.V. All rights reserved.
doi:10.1016/j.jneumeth.2009.06.024

expression was reported to be stable for a year (Bi et al., 2006). We chose rAAV for introducing ChR2 in cultured hippocampal neurons for several reasons. First and foremost, genetic modules introduced into rAAV are less prone to epigenetic gene silencing. Second, long-term expression, from months to years, is achievable. Due to high rate of infectivity, rAAV can be used to introduce multiple genes into the same neurons in pre-selected brain regions (Shevtsova et al., 2005) without epigenetic silencing (Zhu et al., 2007). This broadens the experimental possibilities so that other genes whose products act as biosensors for different signaling systems, such as for calcium (Miyawaki, 2003; Palmer and Tsien, 2006; Wallace et al., 2008) and neurotransmitter release (Miesenbock et al., 1998), could also be introduced into the same neuron using rAAV as the delivery method. This would make it possible to optically record functional neuronal connectivity without the need to use patch pipettes. Moreover, by gene selective knockdown of endogenous protein levels using small interfering RNA (siRNA) (Fountaine et al., 2005), especially under control of the tetracycline-controlled systems (Hasan et al., 2004; Sprengel and Hasan, 2007), it should be possible to correlate how changes in gene activity affect neuronal circuits and animal behavior (Grillner, 2006; Kandel, 2001).

Additionally, the rAAV gene delivery method allows targeting of selective brain regions, which makes it especially powerful for *in vivo* applications. ChR2 has also been targeted to genetically defined populations of neurons through cell-type specific promoters and Cre-dependent constructs to examine neural circuits based on cell types (Atasoy et al., 2008; Liewald et al., 2008). Availability of different AAV serotypes provides additional means to selectively target different neuron types (Burger et al., 2004; Shevtsova et al., 2005; Tenenbaum et al., 2004).

Another feature of rAAV is that it shows low immunogenicity over a long time span (Sun et al., 2002), a key safety criterium that has made rAAV gene delivery the method of choice for therapeutic treatment of animal diseases, including humans. Therefore, rAAV-mediated delivery of ChR2 should not only help to investigate functional brain circuits in living animals but it may also provide a plausible approach to treat neurological diseases which require deep brain stimulation (Gradinaru et al., 2007; Mehrkens et al., 2008; Obeso et al., 1997).

The preceding considerations are general reasons for using rAAV to introduce the ChR2 gene into neurons. Our goal in this paper was to develop the ChR2 method specifically for studying evoked synaptic transmission in mass cultures of dissociated hippocampal neurons.

Dual intracellular recording from pairs of dissociated hippocampal or neocortical neurons is a widely accepted method of studying synaptic plasticity (Arancio et al., 1995; Bi and Poo, 1998; Goda and Stevens, 1996; Kaplan et al., 2003). Such experiments are often done with low density cultures. In one culture method, the substrate that the neurons grow on is sprayed in a mist onto the coverslips, making dots that are less than 1 mm in diameter. Then neurons are plated at low density. The microdots physically limit the neurons' growth so that some microislands end up with just a few neurons or even just two (Bekkers and Stevens, 1991, 1995; Segal and Furshpan, 1990). Within such a microisland, the probability of connection is high, so that it is straightforward to find connected pairs of neurons (Kaplan et al., 2003). In another culture method, neurons and glia are plated at the same time at low density, and this also leads to growth of isolated pairs of neurons (Wilcox et al., 1994).

While the microisland technique makes it easier to record from pairs, culturing healthy neurons becomes more challenging at lower densities. Furthermore, pairs of neurons on microislands tend to be strongly coupled, probably by multiple synaptic contacts (Segal and Furshpan, 1990). Evoked postsynaptic currents are typically hundreds of picoamperes or more, while spontaneous postsynaptic currents ("mini"s) are tens of picoamperes or less (Wilcox et al., 1994). A low calcium solution combined with microperfusion of a high calcium, hypertonic solution (Bekkers and Stevens, 1995) has been used to reduce the amplitude of evoked postsynaptic currents by permitting activation of only a small subset of synapses between two neurons. But without this kind of manipulation, postsynaptic currents evoked in microisland cultures are much larger than those recorded in brain slice experiments.

For these reasons, we have been interested in using mass cultures for synaptic plasticity experiments. These types of cultures are relatively easy to grow and keep healthy, because neurons can be cultured at higher densities. But in our experience, it is difficult to find connected pairs by intracellular recording of randomly chosen neurons, because the probability of connection is low. ChR2 could potentially solve this problem, by allowing the screening of many candidate neurons to find presynaptic partners of a single postsynaptic neuron. We could do this by expressing ChR2 in the culture, and then stimulating presynaptic neurons with a laser while patch recording from a single neuron. If a stimulated neuron is monosynaptically or polysynaptically connected to the recorded neuron, a synaptic response should be observed.

For this purpose, we needed a delivery method for ChR2 that reliably resulted in viable cells, adequate expression levels, and expression during the right time window. We also needed a method of optical stimulation that was spatially precise and reliably evoked action potentials.

In dissociated cultured neurons, experiments on synaptic physiology are typically done between one and three weeks *in vitro* (Arancio et al., 1995; Bekkers et al., 1990; Bekkers and Stevens, 1995; Bi and Poo, 1998; Goda and Stevens, 1996; Gomperts et al., 2000; Kaplan et al., 2003). Earlier than one week, there is little or no synaptic transmission (Gomperts et al., 2000). After three weeks, there is typically spontaneous synchronous bursting (Pasquale et al., 2008; van Pelt et al., 2004a,b), which could interfere with plasticity experiments. For this reason, we were interested in characterizing the expression of ChR2 during this time window. Based on the fluorescence of a ChR2-YFP fusion protein, expression starts at about one week, and is strong after about two weeks *in vitro*. Infected cells looked as healthy as uninfected cells, as they could not be distinguished from each other in phase contrast images.

To characterize the effectiveness of optical stimulation, we performed patch clamp recordings of neurons while simultaneously illuminating them transiently. After two weeks *in vitro*, about 80% of infected cells could be stimulated to generate action potentials using wide-field illumination. Stimulation by laser was more difficult, and depended on the size of the illuminated spot. A 40 μm diameter spot stimulated approximately one third of infected neurons, whereas a 10 μm diameter spot stimulated only one quarter. This demonstrated a trade-off between the fraction of cells that can be stimulated, and the accuracy of spatial localization of stimulation. The luminance of the spot had little effect, if it was above a threshold value. If a cell could be stimulated to fire an action potential, then this response was highly reliable every time it was illuminated.

Our next goal was to investigate the best means of using ChR2 to study synaptic transmission. We performed patch clamp recordings of neurons that were not expressing ChR2, or only weakly, in order to reduce the possibility or magnitude of direct stimulation by light. Then we scanned the laser across multiple locations arranged in a grid. Many types of responses were recorded in the patch clamped neuron, which appeared to be direct, monosynaptic, or polysynaptic. Based on classification of these responses, we propose a criterion for identifying possible monosynaptic pairs of neurons using amplitude, shape, and latency of the recorded currents.

2. Materials and methods

2.1. Preparation of rAAV

The viral expression construct rAAV-P_{hSYN}–ChR2-YFP was constructed by subcloning the ChR2-YFP fragment (Boyden et al., 2005) into an adeno-associated (serotype-2) viral expression cassette with the human synapsin promoter (P_{hSYN}), a woodchuck post-transcriptionalregulatory element (WPRE), and a bovine growth hormone (BGH) polyadenylation sequence (Shevtsova et al., 2005). rAAV was prepared by transfecting HEK293 cells with the plasmid rAAV-P_{hSYN}–ChR2-YFP together with helper plasmids (Grimm et al., 2003), pDp1 (serotype 1) and pDp2 (serotype 2)in a ratio of 3:1 harboring expression cassettes for replicase and capsid proteins. Seventy-two hours after transfection, HEK293 cells were washed once with phosphate-buffered saline (PBS) and collected into 50 ml falcon tubes, pelleted by centrifugation and resuspended in lysis and digestion buffer supplemented with benzonase (Sigma) at 37 °C for 30 min and with NaCl at 50 °C for 30 min. Cell debris was removed by centrifugation at 6000 rpm and clear supernatant was frozen at −70 °C. For harvesting pure virus, the supernatant was thawed on ice and layered on an idoxanol (Progen, Germany) gradient (Auricchio et al., 2001). Centrifugation was done for 60 min, and the virus located on top of the 40% idoxanol layer was removed and placed into a 15 ml falcon tube. To remove salt and further concentrate the virus, the idoxanol gradient fraction was washed three times with PBS and concentrated to a volume of 200–300 μl using Amicon filters (Amersham). Infectious virus titers were determined in primary neuron cultures as described previously (Zhu et al., 2007).

2.2. Primary dissociated cell culture

Dissociated primary cultures of rat hippocampal neurons were prepared in 24-well plates as described previously (Hagler and Goda, 2001). Hippocampi were extracted from P0 rat pups, rinsed three times in HBSS, incubated with an enzyme solution containing 1 mM L-cysteine, 0.5 mM EDTA, 1.5 mM $CaCl_2$, 200 units Papain (Worthington), and 0.1 μg/ml DNAse in a modified HBSS (contains an additional 25 mM HEPES, pH 7.3) for 30–40 min, and then mechanically triturated with a fire-polished pipette. The cells were counted on a hemocytometer and diluted in culture medium containing 6 mg/ml glucose, 1 mM Na–Pyruvate (Invitrogen), 10% fetal bovine serum (Hyclone), 0.1% Mito serum extender (Invitrogen), 2% B27 (Invitrogen), and 1 mM HEPES (pH 7.3) in Basal Medium Eagle (Invitrogen), so that the plating density was 50,000 cells/mL. The cells were plated on 12 mm German glass coverslips (Electron Microscopy Sciences), coated with a mixture of 5.5 mM acetic acid and 0.9 mg/ml rat tail collagen (BD Biosciences). After 2 days, 20 μM Ara-C (Sigma) was added to prevent further growth of glia.

The virus (rAAV-P_{hSYN}–ChR2) was added either to the cell suspension just before plating or 1 day after plating by adding 1–3 μl of solution containing the virus for each well. The culture medium was not changed after adding the virus.

2.3. Electrophysiology

The culture was visualized using an inverted microscope (Olympus IX-70) and a QICam CCD camera (Qimaging). Whole cell recordings of membrane potential and currents were obtained using a patch clamp amplifier (Axon Instruments). The bath solution contained (in mM): NaCl 145, KCl 3, HEPES 10, $CaCl_2$ 3, glucose 8, $MgCl_2$ 2, pH 7.30 as described previously (Bi and Poo, 1998). To prevent washout of the intracellular milieu, we used a perforated patch solution containing (in mM): potassium gluconate 136.5, KCl 17.5, NaCl 9, $MgCl_2$ 1, HEPES 10, EGTA 0.2, pH 7.20 as described previously (Bi and Poo, 1998) with 300 μg/ml Amphotericin-B (Sigma). Data were sampled at 10 kHz and collected using the Matlab XPC target toolbox. Sutter micromanipulators were used to position the patch pipettes.

The holding current for current clamp recordings was set to the leak current, which was defined to be the current measured when the neuron was voltage clamped at −70 mV.

2.4. Optical stimulation

Wide-field stimulation of patch clamped neurons was performed with an unfiltered XCite lamp, attached to the epi-fluorescence illumination port on the microscope.

Timing and synchronization with the electrophysiology for both wide-field and laser stimulation were achieved by triggering a mechanical shutter (Uniblitz) placed between the light source and the microscope. However, the opening time of the shutter did not occur synchronously with the trigger. We measured the time for the shutters to open using a silicon photodiode (Thorlabs). The delay in opening of the wide-field shutter (Model VS35) from the trigger time was measured to be 3.4 ± 0.1 ms (mean ± standard deviation for five measurements), and the delay for the laser shutter (Model VS25) was 3.3 ± 0.04 ms (mean ± standard deviation for five measurements). The reported latencies for the electrophysiological signals were calculated by measuring the time between the point of interest and the shutter trigger signal and then subtracting the mean shutter delay time from this difference.

A guided laser stimulation system was designed using a 30 mW 488 nm solid state laser (Coherent). The laser output was coupled to a fiber optic (Point Source), beam diameter expanded to 3 mm, passed through neutral density filters, directed into galvos (Cambridge Technologies, model 6210H) to move the beam, and sent through a scan lens so that the spot was focused in the image plane of the microscope (Olympus IX-70). A schematic of the optical system is shown in Fig. 3A.

The intensity of the laser measured at the sample ranged from 10 μW to 1 mW. We measured the diameter of the laser spot size by sandwiching a drop of fluorescein between two coverslips and taking an image of the fluorescent excitation produced by the laser spot. We plotted the intensity values across a line centered over the spot. From the resulting profile, we calculated the diameter of the spot as the full width at half maximum (FWHM) intensity. The luminance was calculated using the intensity measurement at the sample, divided by the area of the laser spot, calculated from the FWHM.

To accurately stimulate specific locations in the culture, a map of control voltages for the galvos and the corresponding laser spot location in the image was created at intervals of 100 pixels. Values were interpolated between these points. Custom software was written in Matlab to guide the laser spot to particular spatial locations and control the mechanical shutter.

3. Results

3.1. rAAV mediated delivery of ChR2-YFP into neurons

To monitor the expression levels of ChR2 in neurons, the ChR2 gene was fused to a yellow fluorescent indicator protein (YFP) (Boyden et al., 2005) and cloned into a rAAV expression plasmid with the human synapsin promoter (P_{hSYN}) (Shevtsova et al., 2005) driving ChR2-YFP expression (rAAV-P_{hSYN}–ChR2-YFP) (Fig. 1A). Virus with capsid proteins of the serotype 1 and 2 was prepared as described previously (Zhu et al., 2007). The culture

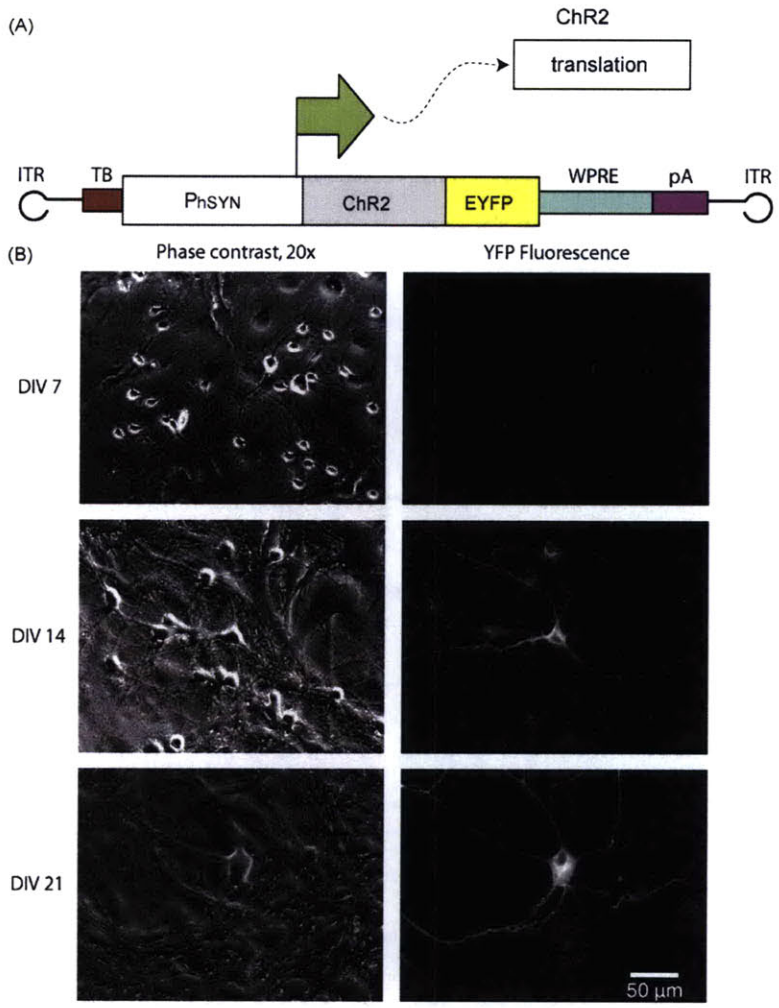

Fig. 1. (A) Expression cassette for rAAV-P_{hSYN} –ChR2. The human synapsin promoter (PhSYN) drives expression of ChR2-EYFP. Labels: synthetic transcription blocker (TB), a woodchuck hepatitis virus posttranscriptional control element (WPRE), polyadenylation signal (pA), inverted terminal repeats of AAV2 (ITR). (B) Left column shows phase contrast images of primary hippocampal culture at DIV 7, DIV 14, and DIV 21, magnified 20×. Right column has the same field of view as the left. The 50 µm scalebar applies to all images. Images were taken using an Excite lamp and YFP filter so that YFP fluorescence could be observed. Exposure time was fixed for all the fluorescence images so that visual comparison could be possible.

was infected with the virus, rAAV-P_{hSYN}–ChR2-YFP, 1–2 days after plating.[1] We observed YFP expression in the culture at 7, 14, and 21 days *in vitro* (DIV). Phase contrast and fluorescence images at 20× magnification are compared in Fig. 1B for these different time points. The exposure time is the same for all fluorescence images (2 s), so that image intensity should be directly proportional to YFP expression. Expression appears to begin around DIV 7, but does not reach high levels until DIV 14.

3.2. Wide-field stimulation of neurons expressing ChR2

We then assessed the effectiveness of wide-field stimulation as a function of days *in vitro*, spanning the time period from DIV 7 to DIV 27. Previous experiments performed on dissociated hippocampal neurons were done between DIV 14 and DIV 28 and made no distinction between different time points in ChR2 expression (Boyden et al., 2005; Schoenenberger et al., 2008).

We performed current clamp recordings of neurons that were visibly expressing YFP (see Fig. 2A for diagram of experiment). We applied the synaptic blockers CNQX, APV, and bicuculline to ensure that responses were due to direct stimulation by light, rather than indirect stimulation through synaptic transmission. The neurons were stimulated with 5 pulses of broadband visible light for 10 ms per pulse. Sample traces from 3 neurons at DIV 7, 14, and 21 are shown in Fig. 2B.

Stimulation was defined as "reliable" if the neuron spiked in response to all 5 pulses of light. We quantified reliability as a function of days *in vitro* (Fig. 2D). The data were grouped so that week 1 included DIV 7 to DIV 13, week 2 included DIV 14 to DIV 20, and week 3 included DIV 21 to DIV 26. In week 1, only 29% of neurons showed reliable stimulation ($n = 7$), consistent with the weak YFP signal reported above. This increased to 71% in week 2 ($n = 14$) and

[1] Previous experiments in hippocampal culture have utilized lentiviral vectors for delivery of ChR2, applied at DIV7 (Boyden et al., 2005; Schoenenberger et al., 2008).

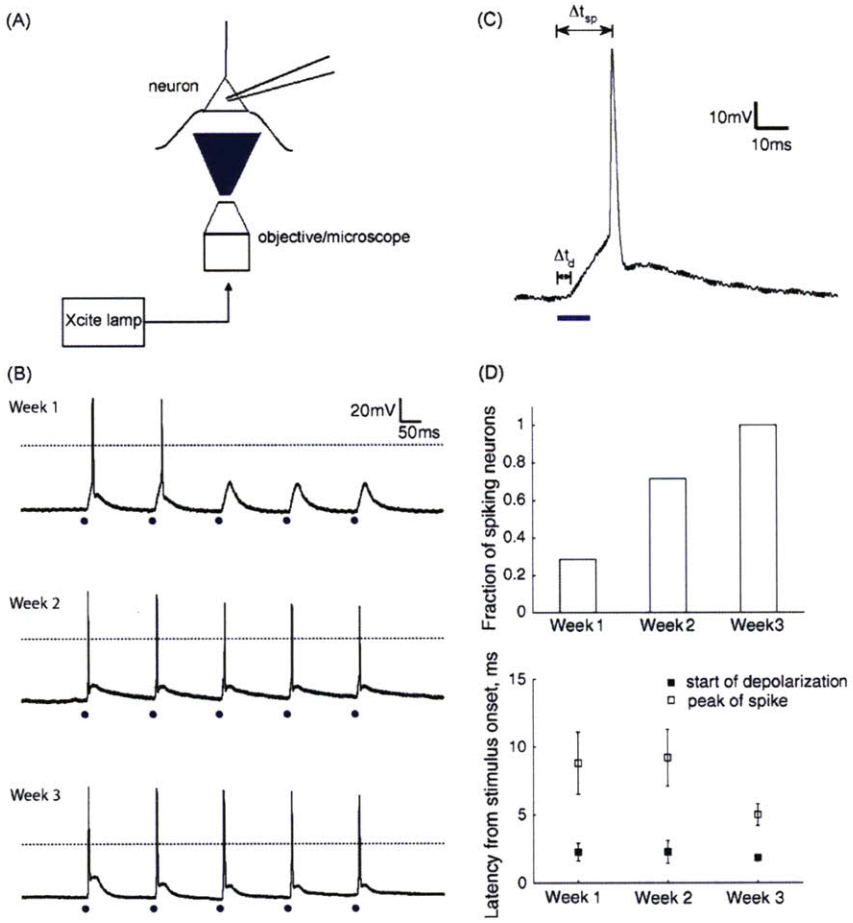

Fig. 2. (A) Schematic of experimental setup showing patched neuron stimulated with widefield illumination. (B) Example recordings from neurons in current clamp from five light stimulations at three different time points in the development of the cultures. The stimulations are indicated with a blue dot and are 10 ms each with frequency 6.25 Hz. Dashed line indicates threshold set at −10 mV, used to determine if neuron fired an action potential or not. (C) Zoomed in example of an action potential that was stimulated by light. The blue line indicates the 10 ms duration of light stimulation. The latency to depolarization, Δt_d, is the time from the onset of light to the beginning of the photopotential. The latency to the peak of the spike, denoted Δt_{sp}, is the time from the onset of light to the peak of the action potential. These measurements are shown in the bottom panel of D for different time points in development. (D) Upper panel shows the fraction of neurons which spike for every photo stimulus for three different age groups (week 1, $n = 7$; week 2, $n = 14$; week 3, $n = 4$). A neuron was considered to spike if for each of five stimuli (shown in B), the neuron fired an action potential. Lower panel shows the average latencies for photostimulation. Open squares indicate mean latency to depolarization within and across neurons; errorbars indicate standard deviation within and across neurons (week 1, $n = 35$ photostimulations; week 2, $n = 70$ photostimulations; week 3, $n = 20$ photostimulations). Solid squares indicate mean latency to the peak of the action potential for the same age groups. The mean latency was calculated from the average spike latency for individual neurons (week 1, $n = 2$ neurons; week 2, $n = 11$ neurons; week 3, $n = 4$ neurons). Error bars denote the standard deviation for the population of neurons. (For interpretation of the references to color in this figure legend, the reader is referred to the web version of the article.)

100% in week 3 ($n = 4$), again consistent with stronger expression levels as observed using fluorescence.

We calculated the mean and standard deviation of the latency from the onset of light to the start of depolarization (Δt_d, see Fig. 2C). As shown in Fig. 2D, for week 1, $\Delta t_d = 2.2 \pm 0.7$ ms ($n = 7$ neurons, 5 photostimulations/neuron); for week 2, $\Delta t_d = 2.3 \pm 0.8$ ms ($n = 14$ neurons, 5 photostimulations/neuron); and for week 3, $\Delta t_d = 1.8 \pm 0.2$ ms ($n = 4$ neurons, 5 photostimulations/neuron). The mean values show that the latencies were about the same for all weeks. The standard deviations are rather small, indicating that the latencies were about the same for all neurons.[2]

We also calculated the mean and standard deviation of the latency from light onset to the peak of the action potential (Δt_{sp}, see Fig. 2C) for neurons which could be reliably stimulated and averaged the mean and standard deviation for the neurons by week. As shown in Fig. 2D, for week 1, $\Delta t_{sp} = 8.8 \pm 2.3$ ms ($n = 2$ neurons); for week 2, $\Delta t_{sp} = 9.2 \pm 2.1$ ms ($n = 11$ neurons); and for week 3, $\Delta t_{sp} = 5.0 \pm 0.8$ ms ($n = 4$ neurons). Judging from the mean latency, which decreased over time, and the standard deviation, the latency to spiking is more variable than the latency to start of depolarization. This is not surprising, given that the latency to spiking is determined by the time to integrate to threshold, and therefore depends on many factors like the amplitude of the ChR2 current and intrinsic properties of the neuron. Previous measurements found that the latency to spiking was 8.0 ± 1.9 ms for DIV 14 hippocampal culture (Boyden et al., 2005), which is comparable to our measurements.

[2] Note that all confidence intervals in this paper are standard deviations, rather than standard errors. This is to give some idea of the variability across a population.

3.3. Laser stimulation

The preceding experiments were performed using wide-field stimulation, which lacks the spatial resolution necessary for finding connected pairs of neurons. In our laser stimulation experiments, we chose to focus on the time period between DIV 14 and DIV 21. This is before spontaneous bursting emerges in mass cultures (Pasquale et al., 2008; van Pelt et al., 2004a,b), and our wide-field experiments suggested that it should be possible to stimulate neurons during this time window.

Again we performed current clamp recordings of neurons, this time stimulating them with a laser. Fig. 3B shows an example of a patched neuron, and the blue dot indicates the location of a typical laser stimulation. For these measurements, we targeted the optical stimulation to the soma. The experiments were performed in the presence of CNQX, APV, and bicuculline to ensure that responses were direct rather than synaptically mediated.

Initially, we tuned the laser spot to be approximately 1 μm in diameter. Since the soma of the neurons varied between 10 and 20 μm in diameter, this spot size would keep the stimulation confined to the soma, resulting in high spatial resolution. While depolarization responses were observed, no spikes were stimulated (data not shown). Turning up the intensity caused saturation of the amplitude of the subthreshold depolarization, but still no spikes were observed.

Then we tried 10 and 40 μm spot diameters, indicated by white circles in Fig. 3B, with various intensity values. For both spot diameters we used a 10 ms laser pulse. If a neuron did not spike, increasing the duration beyond this value did not make any difference. This is consistent with previous experiments showing that the photocurrent decays after about 10 ms of photostimulation (Wang et al., 2007).

The threshold luminance for stimulation was about 500 mW/mm^2,[3]. Below this value, none of the neurons would fire action potentials when stimulated with the 10 μm spot ($n = 4$), and only one response was observed for the 40 μm spot ($n = 5$). For luminance values above this threshold, stimulation with the 10 μm spot was reliable for 20% of neurons ($n = 5$), and with the 40 μm spot was reliable for 33% ($n = 6$) (Fig. 3C, upper panel).

These percentages are lower than for wide-field stimulation. The 40 μm spot illuminated the entire soma and proximal dendrites. Wide-field stimulation also includes more distant sites in the axon and/or dendrites, which could account for its higher success rate.

3.4. Spatial resolution of laser stimulation

We next characterized the spatial resolution of laser stimulation by recording responses in a neuron while illuminating multiple locations arranged in a grid. The grid locations are indicated by the blue circles in Fig. 4A and were spaced approximately 12 μm apart. The locations were stimulated in random order, and the photoresponses were measured. The peak amplitudes of the photoresponses formed a two-dimensional map (Fig. 4B). Again, stimulation was performed in the presence of synaptic blockers.

We estimated the spatial resolution of stimulation by calculating the second moment of distance from the soma, weighted by the amplitude of the map. The square root of this number gave an estimate of the spatial radius of stimulation. The estimation was done separately for subthreshold and spiking responses, and for each spot size. The standard deviation of the radius was also calculated, to characterize the variability across neurons. For the 10 μm spot, the radius of subthreshold responses was 102.4 ± 15.4 μm ($n = 2$), and for the 40 μm spot, the radius of subthreshold responses was 69.5 ± 2.3 μm ($n = 3$). Likewise, the radii of superthreshold responses were as follows: 42.2 μm ($n = 1$) for the 10 μm spot and 33.7 ± 11.6 μm ($n = 2$) for the 40 μm spot. The resolution had little dependence on the size of the laser spot, indicating that the morphology of the neuron could be more important than the spot size in determining the spatial extent of responses. This is perhaps due to activation of ChR2 expressed in the proximal dendrites.

We could probably have obtained better spatial resolution by lowering luminance to the minimum value necessary for producing spikes by somatic illumination, as was shown previously (Schoenenberger et al., 2008). However, it is also important to know the spatial resolution that is possible at luminances above the minimum value.

We might also have obtained better spatial resolution by lowering the spot diameter below 10 μm. However, our experience with the 1 μm spot suggests that better spatial resolution would come only at the cost of drastically reducing the fraction of neurons that can be stimulated reliably.

3.5. Response latencies for laser stimulation

We also measured the latencies from light onset to the peak of the action potentials evoked by laser stimulation targeted to the soma, similar to the measurements reported above for wide-field stimulation. Data were pooled from both 10 and 40 μm laser spots, and various luminances greater than 500 mW/mm^2. For each of three neurons with action potential responses, we plotted the mean and the standard deviation for the latency to the peak response (Fig. 3C, lower panel). The average of the mean latencies across neurons was 7.8 ± 2.6 ms ($n = 3$ neurons). The standard deviation of the mean latency across neurons was greater than the standard deviation of the latency for a single neuron.

We also measured the latency to the start of the depolarization, including both super- and subthreshold responses of 11 neurons. For a given spot size, there was little variability between neurons, so all of the data was lumped together. The mean and standard deviation of the latency were 0.9 ± 0.8 ms ($n = 5$) for the 10 μm spot and 0 ± 0.4 ms ($n = 6$) for the 40 μm spot.

It is not surprising that the latency to spiking is quite variable across neurons since it depends on the time required for the neuron to integrate the ChR2 current to threshold. The latency to response onset is less variable because it does not include this integration time.

The latencies for laser illumination were similar to those for wide-field stimulation, but slightly less. The latencies for wide-field stimulation are useful for comparison to previous experiments reported in the literature (Boyden et al., 2005). The latencies for laser illumination are more relevant to our attempts to find synaptically connected pairs of neurons, which are reported below.

3.6. A latency criterion for distinguishing between direct vs. synaptic responses

Up to now, we have discussed the case of direct stimulation, intracellular recording in the same neuron that is being subjected to laser illumination. To measure synaptic responses, we must record from a different neuron than the one stimulated by the laser. In an ideal experiment, the neuron chosen for intracellular recording would not express ChR2 at all, so there would be no possibility of direct stimulation. We were not able to find such neurons in our cultures, due to the high rate of AAV infection, so we had to settle for recording from neurons with low but nonzero expression levels.

[3] We report luminance value because normalizing by laser spot area calculated from the FWHM provided a clear threshold. Previous results from laser stimulation of single neurons expressing ChR2 were reported for a range of intensity values and spot sizes which were similar to ours (Wang et al., 2007; Schoenenberger et al., 2008).

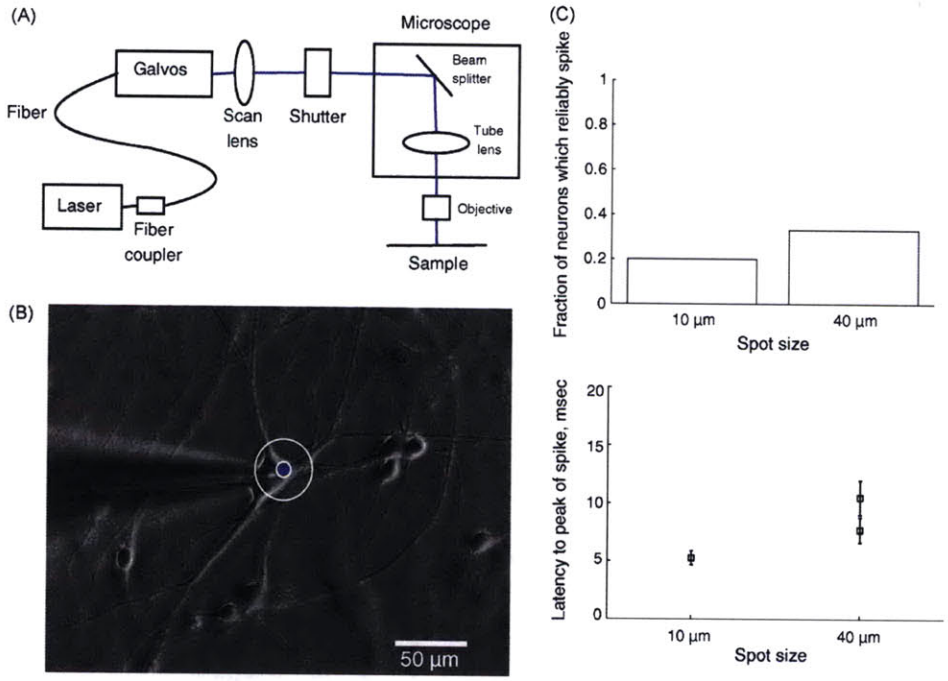

Fig. 3. (A) Optics diagram for laser stimulation. (B) Image of patch clamped neuron at 20× magnification. Blue dot indicates the location of the laser stimulation. The concentric white circles show the size of the 10 and 40 μm diameter spot sizes. (C) Top panel shows the fraction of neurons which spike reliably in response to laser stimulation with luminance greater than 500 mW/mm^2 for the 10 μm ($n = 5$) and 40 μm ($n = 6$) spot diameters. The lower panel shows the average latencies to the peak of the action potential for three neurons which reliably spiked in response to laser stimulation (measurements from $n = 5$ spikes/neuron). The spot diameter is indicated on the x-axis. Error bars denote the standard deviation. (For interpretation of the references to color in this figure legend, the reader is referred to the web version of the article.)

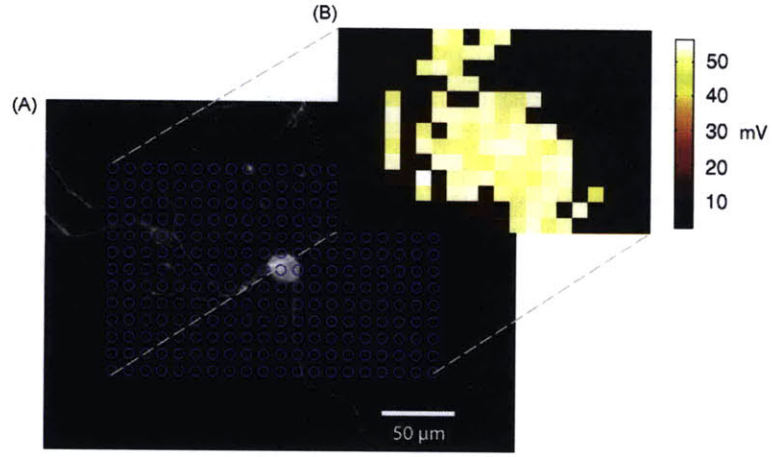

Fig. 4. (A) YFP image of neuron expressing ChR2 at 20× magnification. The blue circles indicate the locations of laser stimulation in a grid around the neuron. (B) Colorcoded map of the photoresponse amplitudes in mV, measured from the neuron pictured in panel A. The numerical value of the amplitudes is shown in the colorbar to the right. The spatial locations in the amplitude map correspond to the grid locations in A as indicated by the dashed lines. The white areas in the amplitude map are locations where the laser stimulated action potentials.

As a consequence of this experimental limitation, there was always the possibility of direct stimulation. Because of the low expression levels, the responses to direct stimulation were weak, and hence could be confused with synaptic responses, if amplitude were the only criterion. However, the results of the previous section suggest that latency can be used to distinguish between direct and synaptic responses. We propose that latencies between 0 and 3 ms indicate direct responses, whereas latencies greater than 8 ms indicate synaptic responses. The latter figure is justified because the latency of a synaptic response should be greater than the latency of spiking in the laser-stimulated neuron, which was measured in the previous section.[4]

[4] There is substantial variability across neurons in the mean latency to spiking. Furthermore, there is some uncertainty in extrapolating the latency to spiking from

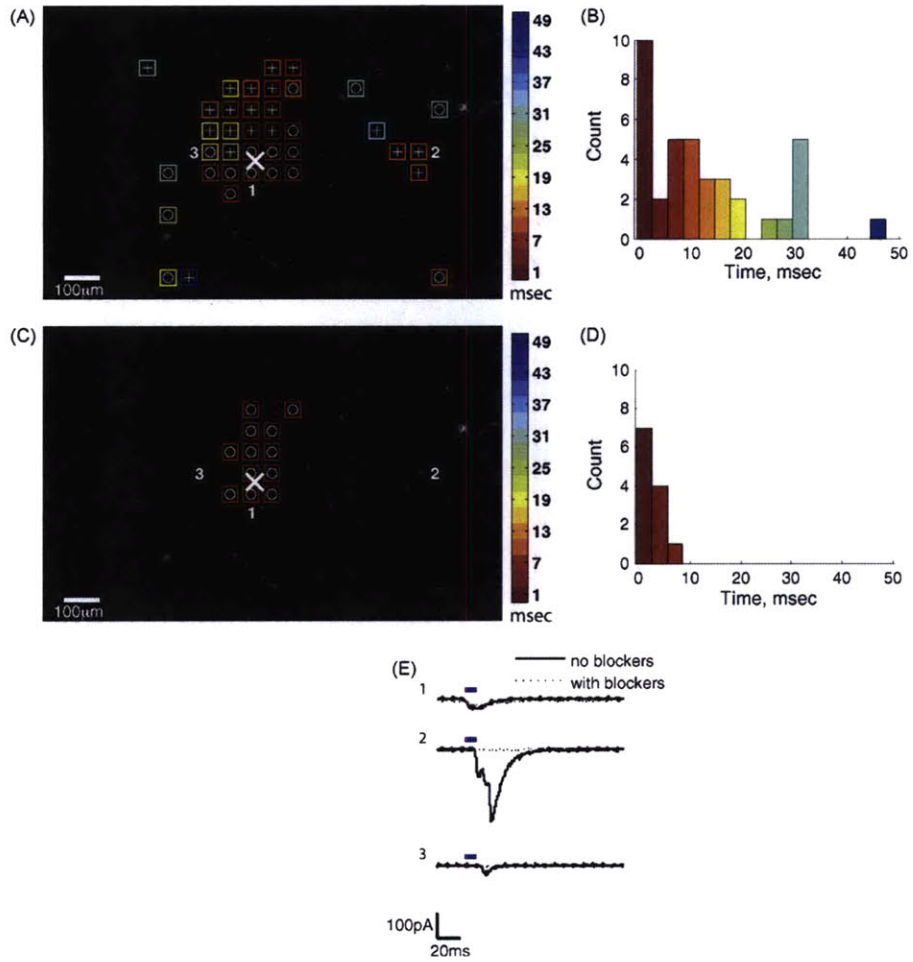

Fig. 5. Image of culture at 4× showing YFP fluorescence (A and C). Overlaid is a map of colored squares indicating the latency from onset of light to the start of the photocurrent. The colorbar to the right indicates the magnitude of the latency in milliseconds. The white (X) marks the location of the patch electrode. The (+) markers indicate a complex response, and the (○) markers indicate a simple response in the induced photocurrent. The numbers overlaid in the images in panels A and C correspond to the plots in panel E. They are example traces of currents induced in the recorded neuron for stimulation occurring at the location indicated by the number. Plots 1 and 3 in panel E are examples of simple responses, and plot 2 is an example of a complex response. Panels B and D contain histograms showing the distribution of latencies. The data for A and B were acquired without synaptic blockers. The data for panels C and D were acquired with synaptic blockers.

3.7. Finding synaptic responses by scanning laser stimulation

To test the criterion proposed above, we scanned a 40 μm laser spot across the neural culture while recording from a neuron in voltage clamp which was expressing ChR2 at a very low level, judging from YFP fluorescence. We stimulated locations in a grid in random order using the laser. The experiments were done both with and without synaptic blockers to distinguish between direct and synaptic responses, and the results were compared with the latency criterion. We also used a 4× objective for a larger field of view containing more possible laser targets.

For two experiments, Figs. 5 and 6 illustrate the locations in the culture at which laser stimulation produces responses in the voltage clamped neuron, along with a histogram of the observed latencies. Initially, only a subset of locations yielded observable responses in the voltage clamped neuron (Figs. 5A and 6A), indicating that the laser stimulation has some spatial selectivity. After the addition of synaptic blockers, this subset shrinks (Figs. 5C and 6C). The locations that remain tend to be closer to the cell body of the recorded neuron, consistent with the idea that the synaptic blockers have eliminated the synaptic responses.

To compare with the latency criterion proposed above, the latencies of responses at the various locations are also histogrammed in Figs. 5B and 6B. The addition of synaptic blockers eliminates the responses with latencies greater than 8 ms, and the responses with latencies less than 3 ms are left intact almost completely (Figs. 5D and 6D). Therefore the latency criterion is consistent with the direct and synaptic responses as distinguished pharmacologically.

3.8. Classifying synaptic responses

While it was straightforward to distinguish between direct and synaptic responses, it was more difficult to distinguish between different types of synaptic responses. We were unable to solve

the case of a neuron with an electrode attached to the case of a neuron with no electrode. Nevertheless, it seems improbable that the latency to spiking could drop below 3 ms, the cutoff value we propose as the criterion for a direct response.

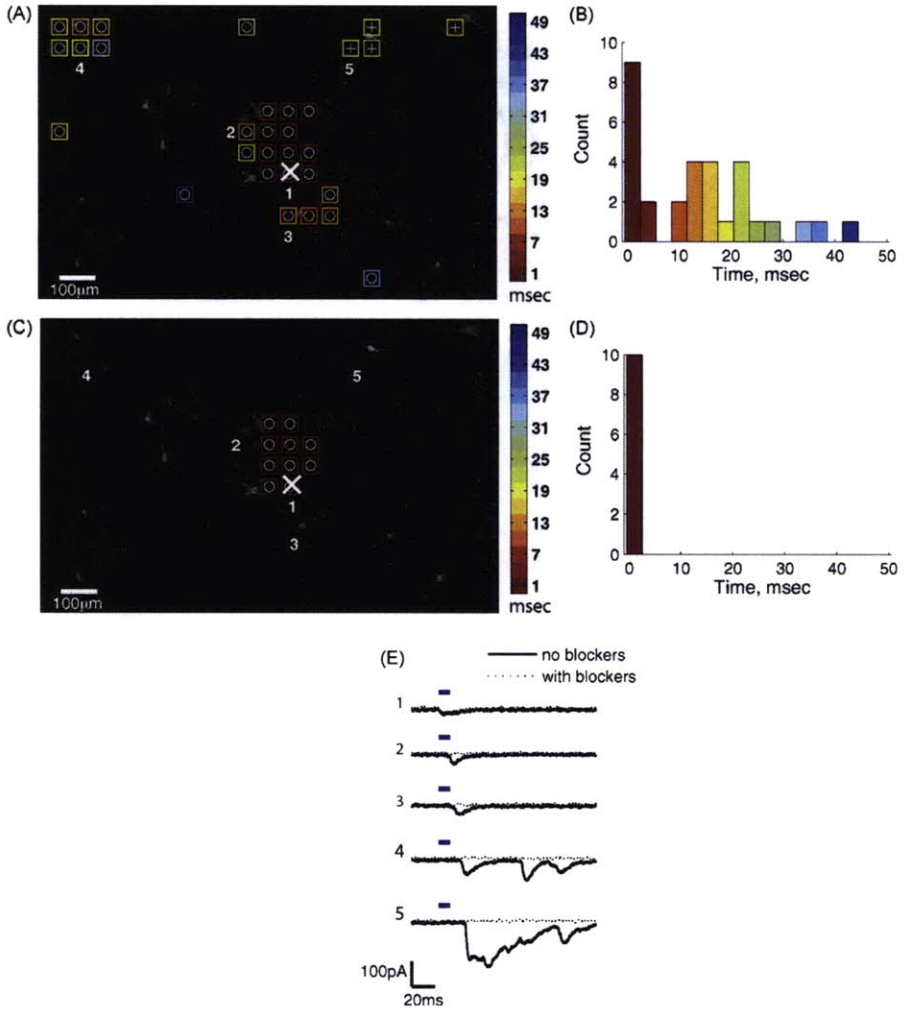

Fig. 6. Another example illustrating the search for synaptic responses. Image of culture at 4× showing YFP fluorescence (A and C). Overlaid is a map of colored squares indicating the latency from onset of light to the start of the photocurrent. The colorbar to the right indicates the magnitude of the latency in milliseconds. The white (X) marks the location of the patch electrode. The (+) markers indicate a complex response, and the (○) markers indicate a simple response in the induced photocurrent. The numbers overlaid in the images in panels A and C correspond to the plots in panel E. They are example traces of currents induced in the recorded neuron for stimulation occurring at the location indicated by the number. Plots 1, 2, 3, and 4 in panel E are examples of simple responses, and plot 5 is an example of a complex response. Panels B and D contain histograms showing the distribution of latencies. The data for A and B were acquired without synaptic blockers. The data for panels C and D were acquired with synaptic blockers.

this problem completely, but we can suggest some tentative criteria.

Figs. 5E and 6E show some voltage clamp responses to laser stimulation. Many responses have a simple shape, but sometimes they are quite complex (Fig. 5E, second trace, and Fig. 6E, fourth and fifth traces). Complex responses are presumably the summation of many synaptic pathways, possibly including both monosynaptic and polysynaptic. Complex responses often have large amplitudes, suggesting that laser stimulation has directly or indirectly caused many neurons in the culture to spike.

We suggest that simple responses with small amplitudes and latencies between 8 and 18 ms are candidate monosynaptic responses. Of course, this criterion cannot be entirely reliable, because the latency to spiking of the stimulated neuron shows substantial variability, as discussed earlier. Narrowing the window to a shorter time interval after 8 ms should reduce the number of false positives, but will also reduce the number of true positives.

4. Discussion

We employed rAAV gene delivery to transfer ChR2 to cultured hippocampal neurons. In wide-field stimulation experiments we found that action potentials could be reliably evoked in many neurons after two weeks *in vitro*, as was previously reported for ChR2 delivered via lentivirus (Boyden et al., 2005; Schoenenberger et al., 2008). We further quantified the fraction of neurons that could be reliably stimulated, as a function of weeks *in vitro*.

We then experimented with laser stimulation, which has superior spatial localization compared to wide-field stimulation. These experiments were similar to those of Schoenenberger et al. (2008), except that we focused on the effectiveness of stimulation. We found a decreased fraction of neurons that could be reliably stimulated to generate an action potential through laser illumination of the soma. For example, after two weeks *in vitro*, the fraction of neurons that could be stimulated dropped to 0.35, from 0.8 for

wide-field stimulation. Reducing the laser spot size produced an even smaller fraction of neurons which spike (Fig. 3c). Therefore the reduced effectiveness of laser stimulation is most likely due to smaller photocurrents produced by stimulation of a smaller number of channels.

Finally, we experimented with the use of laser stimulation at locations away from the soma to evoke synaptic responses. These experiments were similar to the wide-field stimulation experiments of Boyden et al. (2005), but with the possibility of obtaining superior spatial resolution. Although we recorded from cells that expressed low levels of ChR2, photostimulation still produced small inward currents even in the presence of synaptic blockers. Based on amplitude alone, these inward currents due to direct stimulation could be confused with synaptic responses observed in the absence of blockers. However, our measurements showed that direct vs. synaptic responses could be distinguished on the basis of response latency (Figs. 5 and 6). We propose that small inward currents that begin less than 3 ms after light onset are the result of direct stimulation.

It is known that synaptic interactions between cultured hippocampal neurons can be very strong, especially in low density cultures, presumably due to multiple synaptic contacts between pairs of neurons (Bekkers and Stevens, 1995; Segal and Furshpan, 1990; Wilcox et al., 1994). The spiking of a single neuron can be sufficient to drive its postsynaptic targets above the threshold for spiking (Segal and Furshpan, 1990). Therefore, complex synaptic responses due to the superposition of many polysynaptic pathways are often observed. This is in contrast to brain slice experiments, in which stimulation of a single neuron causes subthreshold responses in its postsynaptic targets.

Most of our synaptic currents were about 100 pA or less, which is smaller than the currents observed in microisland cultures of the same age. Nevertheless, many synaptic responses to laser illumination were highly complex in their time courses. This could be due to the recruitment of multiple polysynaptic pathways in parallel, and/or stimulation of more than one neuron. Based on our measurements of latency, we suggest that responses with small amplitudes, simple shapes, and latencies between 8 and 18 ms are candidate monosynaptic responses. This criterion cannot be entirely reliable, but it could be a useful guide.

In comparison to other optical methods for stimulating neurons in culture such as glutamate uncaging (Pettit et al., 1997) and optically stimulating neurons grown on silicon wafers (Colicos et al., 2001; Starovoytov et al., 2005), ChR2 fulfills the requirement for reversible, high-speed, spatiotemporal activation of select neuronal populations (Boyden et al., 2005). Repeated trials of single photon photolysis of caged glutamate could release large amounts of glutamate which might lead to toxicity or non-specific stimulation (Callaway and Katz, 1993). Optically stimulating neurons grown on silicon wafers (Colicos et al., 2001; Starovoytov et al., 2005) was another promising method of non-invasive stimulation, but reliably eliciting action potentials meant increasing illumination intensity, which reduced spatial resolution. Additionally, the neurons could only be stimulated to fire action potentials after three weeks *in vitro* (Starovoytov et al., 2005).

Multi-electrode arrays (MEAs) have also been extensively used to probe cultured neural networks (Corner et al., 2002; Pasquale et al., 2008; van Pelt et al., 2004a,b; Wagenaar et al., 2005), namely to characterize the bursting activity in developing cultured neural networks (van Pelt et al., 2004a,b) and control activity in these networks by stimulating at different electrode sites (Madhavan et al., 2006; Massobrio et al., 2007; Wagenaar et al., 2005). However, the extracellular stimulation from the array suffers from poor spatial localization (Heuschkel et al., 2002) and stimulation artifacts (Wagenaar and Potter, 2004). These stimulation issues have been circumvented by using optical stimulation of caged glutamate to stimulate neurons, while recording exracellular signals viathe MEA (Ghezzi et al., 2008). Laser stimulation of neurons expressing ChR2 could potentially be used in a similar fashion, with the advantage that there would be no accumulation of glutamate in the bath.

Acknowledgement

The authors are grateful for support from the Howard Hughes Medical Institute, the Max Planck Society, and the 2008 NSF Emerging Frontiers in Research and Innovation (EFRI) program. We would like to thank Seungeun Oh for assistance with optics, Jeannine Foley for providing hippocampal culture, Rolf Sprengel and Winfriend Denk for support.

References

Arancio O, Kandel ER, Hawkins RD. Activity-dependent long-term enhancement of transmitter release by presynaptic 3′,5′-cyclic GMP in cultured hippocampal neurons. Nature 1995;376:74–80.

Arenkiel BR, Peca J, Davison IG, Feliciano C, Deisseroth K, Augustine GJ, et al. In vivo light-induced activation of neural circuitry in transgenic mice expressing channelrhodopsin-2. Neuron 2007;54:205–18.

Atasoy D, Aponte Y, Su HH, Sternson SM. A FLEX switch targets Channelrhodopsin-2 to multiple cell types for imaging and long-range circuit mapping. J Neurosci 2008;28:7025–30.

Auricchio A, Hildinger M, O'Connor E, Gao GP, Wilson JM. Isolation of highly infectious and pure adeno-associated virus type 2 vectors with a single-step gravity-flow column. Hum Gene Ther 2001;12:71–6.

Bekkers JM, Richerson GB, Stevens CF. Origin of variability in quantal size in cultured hippocampal neurons and hippocampal slices. Proc Natl Acad Sci U S A 1990;87:5359–62.

Bekkers JM, Stevens CF. Excitatory and inhibitory autaptic currents in isolated hippocampal neurons maintained in cell culture. Proc Natl Acad Sci U S A 1991;88:7834–8.

Bekkers JM, Stevens CF. Quantal analysis of EPSCs recorded from small numbers of synapses in hippocampal cultures. J Neurophysiol 1995;73:1145–56.

Bi A, Cui J, Ma YP, Olshevskaya E, Pu M, Dizhoor AM, et al. Ectopic expression of a microbial-type rhodopsin restores visual responses in mice with photoreceptor degeneration. Neuron 2006;50:23–33.

Bi GQ, Poo MM. Synaptic modifications in cultured hippocampal neurons: dependence on spike timing, synaptic strength, and postsynaptic cell type. J Neurosci 1998;18:10464–72.

Borrell V, Yoshimura Y, Callaway EM. Targeted gene delivery to telencephalic inhibitory neurons by directional in utero electroporation. J Neurosci Methods 2005;143:151–8.

Boyden ES, Zhang F, Bamberg E, Nagel G, Deisseroth K. Millisecond-timescale, genetically targeted optical control of neural activity. Nat Neurosci 2005;8:1263–8.

Burger C, Gorbatyuk OS, Velardo MJ, Peden CS, Williams P, Zolotukhin S, et al. Recombinant AAV viral vectors pseudotyped with viral capsids from serotypes 1,2, and 5 display differential efficiency and cell tropism after delivery to different regions of the central nervous system. Mol Ther 2004;10:302–17.

Callaway EM, Katz LC. Photostimulation using caged glutamate reveals functional circuitry in living brain slices. Proc Natl Acad Sci U S A 1993;90:7661–5.

Clark AJ, Harold G, Yull FE. Mammalian cDNA and prokaryotic reporter sequences silence adjacent transgenes in transgenic mice. Nucleic Acids Res 1997;25:1009–14.

Colicos MA, Collins BE, Sailor MJ, Goda Y. Remodeling of synaptic actin induced by photoconductive stimulation. Cell 2001;107:605–16.

Corner MA, van Pelt J, Wolters PS, Baker RE, Nuytinck RH. Physiological effects of sustained blockade of excitatory synaptic transmission on spontaneously active developing neuronal networks—an inquiry into the reciprocal linkage between intrinsic biorhythms and neuroplasticity in early ontogeny. Neurosci Biobehav Rev 2002;26:127–85.

Ellis J. Silencing and variegation of gammaretrovirus and lentivirus vectors. Hum Gene Ther 2005;16:1241–6.

Fountaine TM, Wood MJ, Wade-Martins R. Delivering RNA interference to the mammalian brain. Curr Gene Ther 2005;5:399–410.

Ghezzi D, Menegon A, Pedrocchi A, Valtorta F, Ferrigno G. A Micro-Electrode Array device coupled to a laser-based system for the local stimulation of neurons by optical release of glutamate. J Neurosci Methods 2008;175:70–8.

Goda Y, Stevens CF. Long-term depression properties in a simple system. Neuron 1996;16:103–11.

Gomperts SN, Carroll R, Malenka RC, Nicoll RA. Distinct roles for ionotropic and metabotropic glutamate receptors in the maturation of excitatory synapses. J Neurosci 2000;20:2229–37.

Gradinaru V, Thompson KR, Zhang F, Mogri M, Kay K, Schneider MB, et al. Targeting and readout strategies for fast optical neural control in vitro and in vivo. J Neurosci 2007;27:14231–8.

Grillner S. Biological pattern generation: the cellular and computational logic of networks in motion. Neuron 2006;52:751–66.

Grimm D, Kay MA, Kleinschmidt JA. Helper virus-free, optically controllable, and two-plasmid-based production of adeno-associated virus vectors of serotypes 1 to 6. Mol Ther 2003;7:839–50.
Hagler Jr DJ, Goda Y. Properties of synchronous and asynchronous release during pulse train depression in cultured hippocampal neurons. J Neurophysiol 2001;85:2324–34.
Hasan MT, Friedrich RW, Euler T, Larkum ME, Giese G, Both M, et al. Functional fluorescent Ca^{2+} indicator proteins in transgenic mice under TET control. PLoS Biol 2004;2:e163.
Hatanaka Y, Hisanaga S, Heizmann CW, Murakami F. Distinct migratory behavior of early- and late-born neurons derived from the cortical ventricular zone. J Comp Neurol 2004;479:1–14.
Heuschkel MO, Fejtl M, Raggenbass M, Bertrand D, Renaud P. A three-dimensional multi-electrode array for multi-site stimulation and recording in acute brain slices. J Neurosci Methods 2002;114:135–48.
Kandel ER. The molecular biology of memory storage: a dialogue between genes and synapses. Science 2001;294:1030–8.
Kaplan MP, Wilcox KS, Dichter MA. Differences in multiple forms of short-term plasticity between excitatory and inhibitory hippocampal neurons in culture. Synapse 2003;50:41–52.
Liewald JF, Brauner M, Stephens GJ, Bouhours M, Schultheis C, Zhen M, et al. Optogenetic analysis of synaptic function. Nat Methods 2008;5:895–902.
Madhavan R, Chao ZC, Wagenaar DA, Bakkum DJ, Potter SM. Multi-site stimulation quiets network-wide spontaneous bursts and enhances functional plasticity in cultured cortical networks. Conf Proc IEEE Eng Med Biol Soc 2006;1:1593–6.
Massobrio P, Baljon PL, Maccione A, Chiappalone M, Martinoia S. Activity modulation elicited by electrical stimulation in networks of dissociated cortical neurons. Conf Proc IEEE Eng Med Biol Soc 2007;2007:3008–11.
Mehrkens JH, Botzel K, Steude U, Zeitler K, Schnitzler A, Sturm V, et al. Long-term efficacy and safety of chronic globus pallidus internus stimulation in different types of primary dystonia. Stereotact Funct Neurosurg 2008;87:8–17.
Miesenbock G, De Angelis DA, Rothman JE. Visualizing secretion and synaptic transmission with pH-sensitive green fluorescent proteins. Nature 1998;394:192–5.
Miyawaki A. Fluorescence imaging of physiological activity in complex systems using GFP-based probes. Curr Opin Neurobiol 2003;13:591–6.
Nagel G, Szellas T, Huhn W, Kateriya S, Adeishvili N, Berthold P, et al. Channelrhodopsin-2, a directly light-gated cation-selective membrane channel. Proc Natl Acad Sci U S A 2003;100:13940–5.
Obeso JA, Rodriguez MC, Gorospe A, Guridi J, Alvarez L, Macias R. Surgical treatment of Parkinson's disease. Baillieres Clin Neurol 1997;6:125–45.
Palmer AE, Tsien RY. Measuring calcium signaling using genetically targetable fluorescent indicators. Nat Protoc 2006;1:1057–65.
Pasquale V, Massobrio P, Bologna LL, Chiappalone M, Martinoia S. Self-organization and neuronal avalanches in networks of dissociated cortical neurons. Neuroscience 2008;153:1354–69.
Petreanu L, Huber D, Sobczyk A, Svoboda K. Channelrhodopsin-2-assisted circuit mapping of long-range callosal projections. Nat Neurosci 2007;10:663–8.
Pettit DL, Wang SS, Gee KR, Augustine GJ. Chemical two-photon uncaging: a novel approach to mapping glutamate receptors. Neuron 1997;19:465–71.
Robertson G, Garrick D, Wilson M, Martin DI, Whitelaw E. Age-dependent silencing of globin transgenes in the mouse. Nucleic Acids Res 1996;24:1465–71.
Robertson G, Garrick D, Wu W, Kearns M, Martin D, Whitelaw E. Position-dependent variegation of globin transgene expression in mice. Proc Natl Acad Sci U S A 1995;92:5371–5.
Schoenenberger P, Grunditz A, Rose T, Oertner TG. Optimizing the spatial resolution of Channelrhodopsin-2 activation. Brain Cell Biol 2008.
Segal MM, Furshpan EJ. Epileptiform activity in microcultures containing small numbers of hippocampal neurons. J Neurophysiol 1990;64:1390–9.
Shevtsova Z, Malik JM, Michel U, Bahr M, Kugler S. Promoters and serotypes: targeting of adeno-associated virus vectors for gene transfer in the rat central nervous system in vitro and in vivo. Exp Physiol 2005;90:53–9.
Sprengel R, Hasan MT. Tetracycline-controlled genetic switches. Handb Exp Pharmacol 2007;178:49–72.
Starovoytov A, Choi J, Seung HS. Light-directed electrical stimulation of neurons cultured on silicon wafers. J Neurophysiol 2005;93:1090–8.
Sun JY, Chatterjee S, Wong Jr KK. Immunogenic issues concerning recombinant adeno-associated virus vectors for gene therapy. Curr Gene Ther 2002;2:485–500.
Tenenbaum L, Chtarto A, Lehtonen E, Velu T, Brotchi J, Levivier M. Recombinant AAV-mediated gene delivery to the central nervous system. J Gene Med 2004;6(Suppl. 1):S212–22.
van Pelt J, Corner MA, Wolters PS, Rutten WL, Ramakers GJ. Longterm stability and developmental changes in spontaneous network burst firing patterns in dissociated rat cerebral cortex cell cultures on multielectrode arrays. Neurosci Lett 2004a;361:86–9.
van Pelt J, Wolters PS, Corner MA, Rutten WL, Ramakers GJ. Long-term characterization of firing dynamics of spontaneous bursts in cultured neural networks. IEEE Trans Biomed Eng 2004b;51:2051–62.
Wagenaar DA, Madhavan R, Pine J, Potter SM. Controlling bursting in cortical cultures with closed-loop multi-electrode stimulation. J Neurosci 2005;25:680–8.
Wagenaar DA, Potter SM. A versatile all-channel stimulator for electrode arrays, with real-time control. J Neural Eng 2004;1:39–45.
Wallace DJ, Borgloh SM, Astori S, Yang Y, Bausen M, Kugler S, et al. Single-spike detection in vitro and in vivo with a genetic Ca^{2+} sensor. Nat Methods 2008;5:797–804.
Wang H, Peca J, Matsuzaki M, Matsuzaki K, Noguchi J, Qiu L, et al. High-speed mapping of synaptic connectivity using photostimulation in Channelrhodopsin-2 transgenic mice. Proc Natl Acad Sci U S A 2007;104:8143–8.
Wilcox KS, Buchhalter J, Dichter MA. Properties of inhibitory and excitatory synapses between hippocampal neurons in very low density cultures. Synapse 1994;18:128–51.
Xia X, Zhang Y, Zieth CR, Zhang SC. Transgenes delivered by lentiviral vector are suppressed in human embryonic stem cells in a promoter-dependent manner. Stem Cells Dev 2007;16:167–76.
Zhang YP, Holbro N, Oertner TG. Optical induction of plasticity at single synapses reveals input-specific accumulation of alphaCaMKII. Proc Natl Acad Sci U S A 2008;105:12039–44.
Zhang YP, Oertner TG. Optical induction of synaptic plasticity using a light-sensitive channel. Nat Methods 2007;4:139–41.
Zhu P, Aller MI, Baron U, Cambridge S, Bausen M, Herb J, et al. Silencing and unsilencing of tetracycline-controlled genes in neurons. PLoS ONE 2007;2:e533.

Chapter 4

Changes in spread of rabies virus in response to perturbations of synaptic vesicle release and neural activity in hippocampal culture

The following is a manuscript.

Changes in spread of rabies virus in response to perturbations of synaptic vesicle release and neural activity in hippocampal culture

May 20, 2010

Abstract

The transsynaptic spread of rabies virus (RV) makes it a powerful tool for mapping circuits of neurons in the brain. Current evidence strongly suggests that the retrograde spread of the virus is restricted to synaptically connected neurons. However, the mechanism which confers synaptic specificity is still unknown. We explored the effects of chronic activity blockade on spread of monosynaptically restricted RV in primary hippocampal culture. Blocking both synaptic vesicle release and activity resulted in increased spread of RV, measured by comparing the ratio of putative presynaptic neurons to postsynaptic neurons in naive conditions to conditions with blockers. Partial block of dynamin-mediated endocytosis with dynasore slightly decreased spread. Although these results may be challenging to interpret in light of homeostatic plasticity changes that may be occuring as a result of chronic activity blockade, the fact that modifying activity is correlated with changes in synaptic spread of RV could be interpreted as further evidence in favor of synaptic restriction of RV.

Introduction

Tracing neural circuits with rabies virus (RV) offers a greatly improved method over conventional tracing techniques. Available evidence strongly argues for the specficity of viral spread to synaptically connected neurons[27, 24, 12]. Additionally, the ability of the virus to rapidly replicate within a neuron allows for amplification of signal [31, 14, 28, 6]. However, the mechanism which confers exclusivity of viral spread between synaptically connected neurons is still in question.[4] Elucidating such a mechanism would bolster the use of RV as a tracing tool, since it would ensure that neurons labeled via infection with RV were synaptically connected.

The main evidence for synaptic restriction of RV comes from previous studies tracing model systems. In these studies, the number of infected neurons within

a nucleus did not increase with time and fibers of passage passing through an infected nucleus did not become infected with RV, implying that there was no local spread of the virus. [27, 28, 29, 12, 24]. Additionally, electrophysiological verification of synaptic connectivity of neurons in slice, labeled with monosynaptically restricted RV, confirms transsynaptic labeling [32].

One explanation for synaptic restriction is that the receptors to which RV particles bind to gain entry into a neuron could potentially be localized to synapses[29, 15, 4]. In contrast, experiments in hippocampal culture show that RV particles bind to the soma and dendrites of cultured neurons [16]. This suggests that there could be non-synaptic specific spread of the virus. To counteract that idea, glial sheathing has been proposed as a way of preventing viral spread into the extracellular matrix [4].

The question of structural constraints on RV spread, as well as potential synaptic mechanisms for viral spread can be addressed in hippocampal culture. RV travels retrogradely, from postsynaptic to presynaptic neurons [12]. Synaptic transmission from a presynaptic neuron to a postsynaptic neuron is one of the main determinants of connectivity. If spread of RV is indeed restricted to synaptically connected neurons, we hypothesize that altering synaptic vesicle release could produce changes viral spread. In particular, blocking synaptic vesicle release or compensatory endocytosis of synaptic vesicles following release could impede viral spread. Alternatively, spread of RV could depend on postsynaptic activity.

To test these hypotheses, we needed a system where we could measure the populations of pre- and post- synaptic neurons. Using monosynaptically restricted RV would allow targeting of a population of initial host neurons, with viral spread limited to neurons which were putatively one synapse away [32], preventing mass infection of the entire culture. The populations of pre- and post- synaptic neurons could be distinguished by different fluorescent labels and counted using image analysis.

Estimating the populations of putative pre- and post-synaptic neurons required imaging whole coverslips of hippocampal culture. Because we started with a small number of postsynaptic neurons that was greater than 1, the locations of their putative presynaptic partners were unknown. Imaging as large of an area as possible would hopefully minimize that confound.

Calculating the ratio of putative presynaptic to postsynaptic neurons provided a measure for comparing the effects of our manipulations. Due to the large number of images acquired for each coverslip, we developed an image analysis pipeline to automate counting neurons. We trained a convolutional neural network to segment neuron somata in DIC images to obtain a total count of the neurons in the culture and counted neurons expressing fluorescent labels using bandpass filtered images.

Here we report the successful use of monosynaptically restricted RV to label clusters of neurons in primary hippocampal culture. Surprisingly, we found that application of synaptic vesicle release blockers botulinum toxin - A (BoNT/A) and tetanus toxin (TeNT) [21, 9] increased the amount of RV spread. We also tested the effect of activity blocker tetrodotoxin (TTX) combined with synaptic

blockers APV, CNQX, and Bicuculline to quench postsynaptic activity and found that this manipulation increased RV spread as well. Applying a partial block of dynamin-dependent endocytosis using dynasore [19] impeded the spread of the virus, although not in a statistically significant way.

Our results could potentially be explained by changes to the underlying structure of the network via homeostatic plasticity mechanisms. Even so, that the spread of RV could reflect these changes provides another confirming piece of evidence for the synaptic restriction of RV.

Methods

Constructs for monosynaptically restricted RV

The plasmid pUB-ETB was constructed by de novo synthesis of a tricistronic open reading frame consisting of three genes coding for EGFP, the TVA transmembrane isoform [18], and the SAD B19 glycoprotein [5] separated by the foot and mouth disease virus and Thosea asigna virus 2A elements [23], which was cloned into the expression vector pUB-GFP [17] under the control of the ubiquitin C promoter.

High titer stocks of G-deleted RV coding for mTagBFP [22], pseudotyped with the avian sarcoma and leukosis virus subgroup A envelope protein (RV-4BFP(EnvA)), were made according to [33].

Primary hippocampal culture

P1 rat hippocampi were extracted and solutions were prepared as described previously [8]. All animals were treated humanely, in accordance with the MIT Committee on Animal Care policies. Hippocampi were collected with dentate gyrus removed and cut into small ($\approx$ 1 mm) pieces in a dissection solution containing 25 mM HEPES in Hank's Balanced Salt Solution (HBSS), pH 7.3. These pieces were dissociated for culture by incubating the tissue for 30-40 min at 37°C in HBSS containing 1 mM L-cysteine, 0.5 mM EDTA, 1.5 mM $CaCl_2$, 20 U/ml Papain (Worthington), and 0.1 μg/ml DNAase. The enzymatically dissociated tissue was rinsed 3 times in culture medium containing 6 mg/ml glucose, 1 mM Na-Pyruvate (Invitrogen), 10% fetal bovine serum (Hyclone), 0.1% Mito serum extender (Invitrogen), 2% B27 (Invitrogen), and 1 mM HEPES in Basal Medium Eagle (Invitrogen), pH 7.3 and then mechanically triturated with a fire polished plastic pipette in culture medium. The cell suspension was diluted so that the plating density was approximately 200K cells/ml. The neurons were plated on 12 mm round glass coverslips coated with 0.5 mg/mL rat tail collagen and 4 μg/ml poly-D-lysine in a 24-well plate. After 2 days, 20 uM Ara-C (Sigma) was added to prevent further growth of glia.

Transfection, infection, and fixation

Primary hippocampal cultures were transfected with pUB-ETB at DIV 7 using Invitrogen's calcium phosphate transfection kit, in a manner similar to [11]. Calcium phosphate precipitate containing the pUB-ETB plasmid was prepared by combining 10 μL 2M CaCl2 with 10 μg pUB-ETB and 80 μL H2O. The DNA solution was added dropwise into 100 μL 2x HeBS, bubbled using a 1 mL pipette, and incubated at room temperature for 25 min to form calcium phosphate precipitate. Cultures were transfered to DMEM with no L-glutamine (Invitrogen) and incubated for 5-7 min before adding 15-20 μL (0.75-1 μg pUB-ETB) precipitate. The cultures were incubated with precipitate for 20 min at 37^{o}C, then rinsed 3 times in pre-equilibrated DMEM, incubating for 10 min after each rinse. After the last rinse, cultures were returned to original culture medium.

Twenty-four hours after transfection with pUB-ETB (DIV 8), 1-2 μL of RV-4BFP(EnvA) was added to the medium. For activity manipulations, a combination of activity blockers, vesicle blockers, or 10 μM Dynasore (Sigma) were added before infection with RV-4BFP(EnvA). The activity blockers included 1 μM TTX (Sigma), 100 μM APV (Sigma), 10 μM CNQX (Sigma), and 10 μM Bicuculline (Tocris), and the vesicle release blockers included 13-26 nM BoNT/A (Sigma) and 10 nM TeNT (Sigma). Four to six hours after RV infection, the medium was replaced with either fresh medium for baseline conditions or medium containing the previously listed drug concentrations.

Control cultures (no manipulations) were subjected to sham calcium phosphate transfection (no precipitate added) and received the same medium changes at the times described above. For the medium exchange control, medium was collected from pUB-ETB transfected, RV-4BFP(EnvA) infected culture 24 hours after the first medium exchange and added to naive culture.

Twenty-four to 48 hours after RV infection, the cultures (DIV 9) were transferred to 4% paraformaldehyde in PBS for 20min at room temperature for fixation., followed by 3 - 10 min rinses in PBS. Coverslips containing cultures were inverted onto slides containing a drop of Prolong Gold Anti-fade mounting medium (Invitrogen).

Image aquisition

Tiled widefield images of the coverslips at 10x magnification were aquired using Slidebook software (Intelligent Imaging Innovations) controlling an Olympus BX61 with motorized stage (Prior). Tilings ranged in size from 12x14 to 16x21 and were acquired at full 1040x1392 pixel resolution of a 12 bit QiCam cooled CCD camera (QImaging) with 5% overlap. Each of three channels were exposed consecutively for each tile. We used DAPI (Semrock DAPI-5060B-OMF) and FITC (Chroma 41017) filter cubes for widefield fluorescence excitation and emission with a X-Cite light source. Exposure times were the same for all coverslips as follows: widefield differential interference contrast (DIC) channel, 30 ms; DAPI channel, 5 s; FITC channel, 5 s. Slidebook's autofocus function was

applied using the DIC channel with a 30 msec exposure. Images were streamed to disk in Slidebook format, then exported as TIFs.

Image analysis

Neurons in DIC images were counted using custom segmentation software written in Matlab. A convolutional network (CN) classifier [10] with a field-of-view of 55x55 pixels was trained on a test set using hand labeled neuron somas until it achieved a 3.5% pixel classification error. Images were rescaled to have pixel intensity values with 0 mean and unit standard deviation and passed through the network. CN output was filtered using a gray scale morphological image opening with a disk structuring element of radius 8 pixels. This filtered version of the CN output was thresholded at 0.8, creating a binary image. Connected components corresponded to neuron locations and were counted (N_{DIC}) using Matlab.

To count BFP expressing neurons, DAPI channel images were bandpass filtered using guassian filters with 7 pixel standard deviation to detect BFP expressing neuron somas and 60 pixel standard deviation to smooth the background. The filtered images were thresholded and connected components counted as the number of BFP neurons (N_{BFP}). Since we were only interested in counting GFP expressing neurons which were also expressing BFP, we used the BFP mask to find the number of GFP expressing neurons (N_{GFP}) in the FITC channel images, defined as having a mean intensity value above threshold for a given connected component in the BFP mask.

All images were manually reviewed for large artifacts which were inadvertently detected by the image processing algorithms and the counts for these images were hand corrected. Addtionally, the images were cropped to exclude overlap in the image tiling to prevent overcounting, and fluorescent images were shifted so that they aligned with DIC images.

The proportion of BFP expressing neurons and GFP expressing neurons were calculated as $\frac{N_{BFP}}{N_{DIC}}$ and $\frac{N_{GFP}}{N_{DIC}}$, respectively. The presynaptic/postsynaptic neuron ratios were calculated as follows: $\frac{N_{BFP}-N_{GFP}}{N_{GFP}}$. Statistical comparisons between different experimental conditions were performed using ANOVA. Tests of significance between conditions were performed using Tukey-Kramer post-hoc analysis.

Results

Monosynaptically restricted RV infection and spread in primary hippocampal culture

It was not immediately obvious that observing RV infection in hippocampal culture would be feasible due to the dense interconnectivity of culture. Likewise, the possibility that RV would spread indiscriminately as in non-neuronal cell culture was also a potential issue. We tested monosynaptically restricted

RV by transfecting hippocampal cultures with the plasmid pUB-ETB, which contained genes coding for eGFP, ASLV receptor TVA, and B19G RV glycoprotein and infected with G-deleted, EnvA pseudotyped RV coding for mTagBFP (RV-4BFP(EnvA)).

First we observed eGFP expression in a subset of neurons following calcium phosphate transfection of the culture. To ensure that this was also evidence of functional TVA receptor expression and B19G (RV glycoprotein) for viral transcomplementation, we infected transfected cultures and wildtype cultures with RV-4BFP(EnvA). We expected that neurons infected with RV-4BFP(EnvA) would be evidenced by BFP expression. Twenty-four hours after RV-4BFP(EnvA) infection of pUB-ETB transfected cultures, we observed neurons expressing both BFP and GFP as well as neurons expressing only BFP, indicating successful infection of TVA expressing neurons with pseudotyped virus. (Figure 1) Infection of wildtype cultures resulted in a negligible number of BFP expressing neurons, providing evidence that pseudotyped virus could not infect wildtype neurons and that the BFP neurons observed in the transfected culture were the result of infection from successfully transcomplemented RV-4BFP(EnvA) with B19G.

In pUB-ETB transfected cultures, BFP expressing neurons were primarily clustered in regions of the culture which had GFP expressing neurons, indicating that there was a spatial correlation between the locations of the initially infected host neurons and the subsequently infected secondary population. To rule out the possibility that we were observing non-specific spread of transcomplemented virus into the culture medium, we removed medium from cultures which were transfected with pUB-ETB and infected with RV-4BFP(EnvA), containing neurons expressing BFP (evidence of synaptic spread), and transferred this medium to naive cultures. Again, we observed negligible BFP expression in these controls as compared to the experimental condition.

Measure of RV spread

To quantify our observations, we fixed and mounted the coverslips and imaged them in widefield tilings using Slidebook's automated image collection process. Figure 2 shows an example coverslip (14x17 tiling) and a schematic of the analysis used to count the neurons. An average of 250 locations were imaged for each coverslip, resulting in an average of 750 images to process for each coverslip after taking the 3 channels imaged into account. For the control conditions, we needed to count the total number of neurons on the coverslip and the number of BFP expressing neurons to statistically compare the differences in BFP expression. For the experimental manipulations, we also needed to count the number of GFP neurons.

We generated the total count of neurons from DIC images. First we trained a convolutional network to segment somas in DIC images by using a handlabeled training set of images. The network was trained until the classification error was ~3.5%. The output of the network was a probability map for the likelihood of pixels being in or out of a soma. Figure 2 shows example output of the

CN. To convert this grayscale map into a binary image, we performed a gray scale opening on the CN output and thresholded the resulting image, creating a binary image. We counted the connected components in the binary image and used this as our count of DIC neurons. We evaluated this analysis using a test set of 10 images. The opened output of the CN detected 76% of the neurons correctly with a false positive rate of 20.3%.

To count BFP expressing neurons (N_{BFP}), we bandpass filtered BFP images and applied a threshold, creating a binary mask. The connected components in this mask corresponded to locations of the BFP neurons and were counted We used this mask to search for GFP expressing neurons in the GFP images, since this would ensure that the GFP expressing neurons were also expressing BFP. (These were the putative postynaptic neurons.) We calculated the mean intensity in the GFP channel for each of the regions of interest in the BFP mask. Regions with average above the GFP threshold were counted as a GFP/BFP expressing neuron with the total number denoted by N_{GFP}. The proportion of BFP neurons relative to the entire culture was calculated as Nbfp/Ndic and the proportion of neruons expressing BFP and GFP was calculated as $\frac{N_{GFP}}{N_{DIC}}$. The number of putative presynaptic neurons was calculated as N_{pre}=N_{BFP}-N_{GFP}, and the ratio of presynaptic to postsynaptic neurons was calculated as $\frac{N_{pre}}{N_{post}}=\frac{N_{BFP}-N_{GFP}}{N_{GFP}}$. All fluorescent images were hand verified to correct for identification of large artifacts.

Quantification of control conditions

We used the measures described in the previous section to quantitatively compare the control conditions. Since we were searching for spurious RV infection, we quantified the proportion of BFP expressing neurons relative to the total number of neurons on the coverslip in each condition. We computed this ratio for each coverslip and averaged over all coverslips for each condition. The means were compared for statistical significance using ANOVA with Tukey-Kramer post hoc comparisons.

Cultures transfected with pUB-ETB and subsequently infected with RV-4BFP(EnvA) (n=6) had a higher rate of BFP expression than 3 other control conditions, which was statistically significant with p=0.0001. These other conditions included sham transfection and no RV infection (nothing) (n=2), culture with sham transfection followed by infection with RV-4BFP(EnvA) (RV only) (n=3), and culture containing medium from pUB-ETB transfected, RV-4BFP(EnvA) infected cultures (medium exchange) (n=2). Figure 3 contains a bar plot indicating the mean BFP proportion for these conditions with error bars denoting standard error. The 3 control conditions were not significantly different from each other.

This quantification confirms our observation that EnvA pseudotyped RV infects only pUB-ETB expressing neurons and that virus released from the initial host infection is not present in the bulk medium. This potentially rules out non-specific local spread of RV in hippocampal culture.

Effects of activity manipulations on RV spread

We tested our hypothesis that blocking synaptic vesicle release would affect the spread of RV by applying a cocktail of 13-26nM BoNT/A and 10nM TeNT (toxins) to inhibit both glutamatergic and GABAergic vesicle release [2, 30, 21, 9]. These blockers were added to cultures transfected with pUB-ETB immediately before infection with RV-4BFP(EnvA). We compared this to the effects of two other activity manipulations: 10uM of dynamin-mediated endocytosis blocker Dynasore (Dynasore) and a combination of activity blockers 1uM TTX, 100uM APV, 10uM CNQX, and 10uM Bicuculline (blockers). Dynamin is required for bulk retrieval of synaptic vesicles in hippocampal culture, for which Dynasore provides a dose dependent blockade [19]. If spread of RV depends on synaptic vesicle recycling, we expect this manipulation would decrease the number of secondary neurons infected with RV. We also applied action potential blocker TTX with a combination of synaptic blockers APV, CNQX, and Bicuculline to test the hypothesis that viral spread could be dependent on postsynaptic activity.

For all of these conditions, we observed infection of pUB-ETB transfected neurons as well as spread to other neurons, evident by expression of BFP only. Qualitatively, there appeared to be more BFP expressing neurons in cultures treated with activity blockers than in the other conditions, and fewer BFP expressing neurons in the two synaptic vesicle treatments. Images representative of areas with BFP clusters are shown in Figure 1. We quantified these observations using the counting method described above. Figure 4A shows the relative proportions of BFP and GFP expressing neurons averaged over coverslips for the control condition (n=6), toxins (n=5), Dynasore (n=5), and blockers (n=6). The height of the bars indicates the mean proportion of neurons expressing BFP (blue bars) and GFP + BFP (cyan bars), calculated by counting the number of neurons for each case and dividing by the total number of neurons on a coverslip. These numbers were then averaged across coverslips. Error bars denote standard error.

To determine if there was a difference in amount of viral spread among these conditions, we computed the ratio $\frac{N_{pre}}{N_{post}}$ for each coverslip and averaged over all coverslips for the control condition and 3 manipulations. We found that the $\frac{N_{pre}}{N_{post}}$ increased for both the blocker and toxin conditions indicating increased RV spread (Figure 4B). These increases were statistically significant compared to the control condition (ANOVA, p=0.002, with post-hoc Tukey-Kramer comparison). There was a slight decrease in amount of spread for the Dynasore condition, but this was not statistically significant.

Discussion

We tested the activity dependence of transynaptic RV spread in primary hippocampal culture using monosynaptically restricted, pseudotyped RV. This system allowed us to target the initial RV host infection to a defined population of neurons and restrict transsynaptic spread to neurons which were putatively one

synapse away[32]. This was important for measuring changes to spread, since having well-defined populations of inital infections and secondary infections provided a basis for comparison. By counting the number of neurons which were initially infected by RV and comparing to the number of neurons which were infected by transsynaptic spread from this initial group, we could compare the effects of activity manipulations.

Our results that blocking synaptic vesicle release and blocking activity increased RV spread were surprising, given our intial hypothesis that they might decrease spread. There are several possible explanations for these observations. The wealth of literature on homeostatic plasticity suggests that our chronic blockade of activity could have induced modifications via synaptic scaling [26, 25, 20]. How increases in quantal size could mechanistically be related to an increase in the number of neurons to which RV spreads is unclear. Alternatively, our results could be explained by an increase in the number of spines which might lead to additional presynaptic neuron contacts. However, this possibility seems unlikely, given the age of culture we used (DIV 7-9). Increases in spine density in response to chronic activity blockade are reported for cultures older than DIV 18 [34] and acute slices from rats between P20-22 [13].

That spread of RV was slightly impeded by partial block of dynamin-mediated endocytosis [19] corroborates evidence that RV particles are endocytosed through acidified endosomal compartments [16]. We were unable to increase the dose of dynasore to completely block dynamin-mediated endocytosis due to negative effects on the health of the culture for the prolonged application period.

The increase in spread due to application of both BoNT/A and TeNT has a less clear interpretation. TeNT blocks GABAergic transmission in the hippocampus and is thought to induce epileptic glutamatergic activity [1]. Coapplication with BoNT/A should counteract this effect by blocking excitatory synaptic transmission[30]. That we did not observe decreased spread of RV by turning off all synaptic transmission implies that RV spread could be independent of synaptic transmission.

That the activity dependent manipulations had a statistically relevant effect on the amount of viral spread suggests that synaptic activity, as well as neuronal activity, are related to spread of RV, although the mechanism remains unclear. That changes in RV spread were correlated with modifications to connectivity and activity of neurons provides additional circumstantial evidence for synaptic restriction of spread. Further experiments, such as genetically targeting inward-rectifying potassium channels to the population of postynaptic neurons to selectively decrease activity in the initial host neurons [3] or selectively inactivating clathrin-mediated endocytosis [7] could provide more resolution on the matter.

Figures

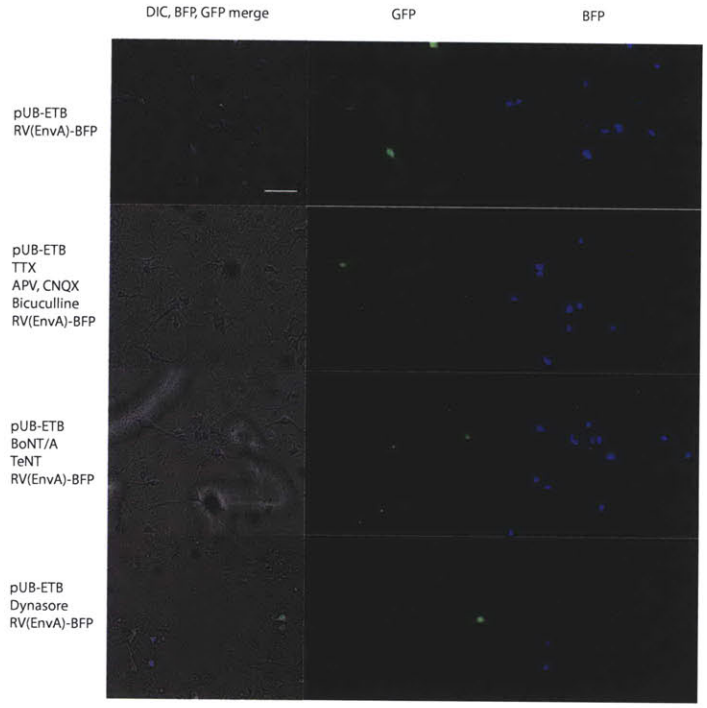

Figure 1: Images of culture transfected with pUB-ETB and infected with RV-4BFP(EnvA). The rows contain images of the culture for each manipulation. Images which had representative BFP clusters were selected. The first column displays 10x DIC image with overlays of the FITC (GFP) and DAPI (BFP) channels for comparison. The second column and third columns show the FITC and DAPI channels separately. The scale bar is 25 μm.

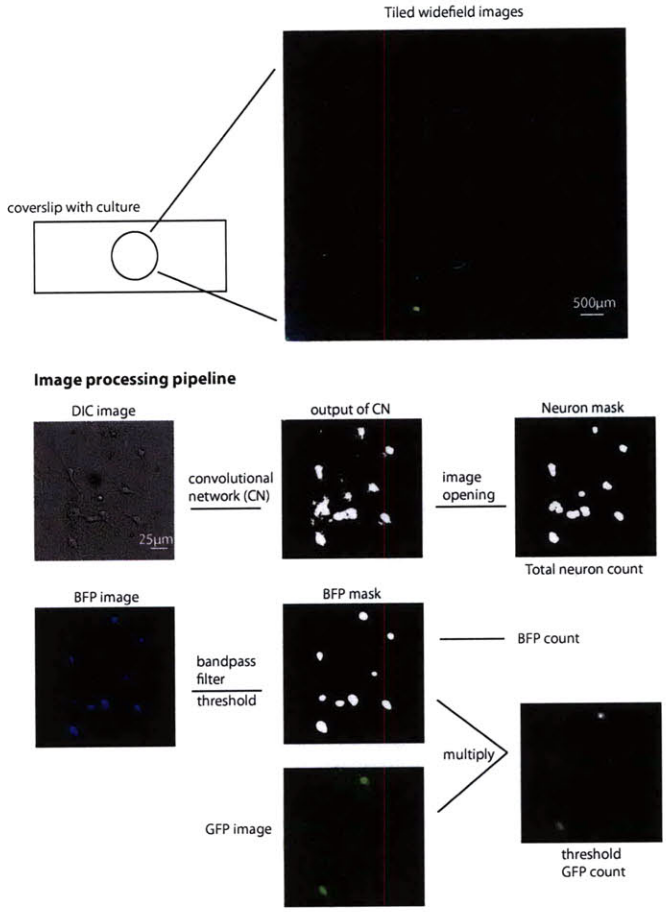

Figure 2: Schematic of data collection and analysis. Coverslips were imaged in widefield tilings. Example image is a 14x17 tiling from a pUB-ETB transfected, RV-4BFP(EnvA) infected culture. Below is the image processing pipeline with example output shown for each step. To count all of the neurons on a coverslip, we used a convolutional network, followed by image opening, and thresholding. BFP neurons were counted by bandpass filtering DAPI images, thresholding to create a mask. GFP neurons expressing BFP were counted using the BFP mask to extract GFP fluorescence values from the FITC channels which were thresholded to produce the GFP count.

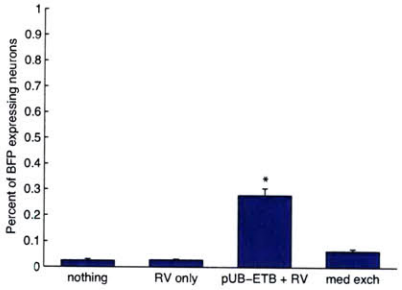

Figure 3: Percent of neurons in culture expressing BFP for control conditions. The height of the bars indicates the fraction of BFP expressing neurons for each coverslip averaged for each condition, and error bars denote standard error. pUB-ETB transfected, RV-4BFP(EnvA) infected cultures had a larger proportion of BFP expressing neurons which was statistically significant compared to control conditions. (ANOVA, p=.0001 with Tukey-Kramer post hoc comparison)

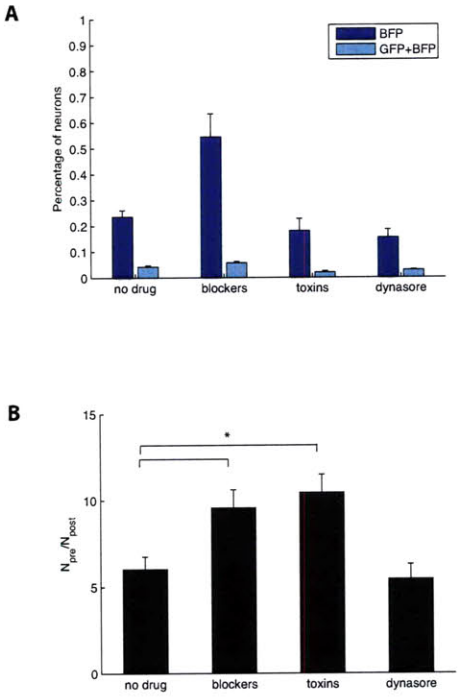

Figure 4: Statistical comparison of activity manipulations to cultures transfected with pUB-ETB, infected with RV-4BFP. (A) Percent of neurons expressing BFP indicates the population of RV infected neurons (blue bars), and the percent of neurons expressing both BFP and GFP (cyan bars) indicates the population of initial host infections. To compare the amount of spread from the initial host infection, the ratio $\frac{N_{pre}}{N_{post}}$ is shown in (B) for all conditions. The amount of spread increased significantly for the conditions where blockers (TTX, CNQX, APV, and Bicuculline) and toxins (BoNT/A and TeNT) were applied. Application of dynasore decreased spread slightly but this decrease was not statistically significant (ANOVA, p=0.002, with post-hoc Tukey-Kramer comparison).

References

[1] G Bagetta and G Nisticò. Glutamate transmission is involved in the mechanisms of neuronal degeneration produced by intrahippocampal tetanus toxin in rats. *Toxicol Lett*, 64-65 Spec No:447–53, Dec 1992.

[2] Thomas Binz and Andreas Rummel. Cell entry strategy of clostridial neurotoxins. *J Neurochem*, 109(6):1584–95, Jun 2009.

[3] Juan Burrone, Michael O'Byrne, and Venkatesh N Murthy. Multiple forms of synaptic plasticity triggered by selective suppression of activity in individual neurons. *Nature*, 420(6914):414–8, Nov 2002.

[4] Edward M Callaway. Transneuronal circuit tracing with neurotropic viruses. *Curr Opin Neurobiol*, 18(6):617–23, Dec 2008.

[5] K K Conzelmann, J H Cox, L G Schneider, and H J Thiel. Molecular cloning and complete nucleotide sequence of the attenuated rabies virus sad b19. *Virology*, 175(2):485–99, Apr 1990.

[6] L W Enquist. Exploiting circuit-specific spread of pseudorabies virus in the central nervous system: insights to pathogenesis and circuit tracers. *J Infect Dis*, 186 Suppl 2:S209–14, Dec 2002.

[7] Björn Granseth, Benjamin Odermatt, Stephen J Royle, and Leon Lagnado. Clathrin-mediated endocytosis is the dominant mechanism of vesicle retrieval at hippocampal synapses. *Neuron*, 51(6):773–86, Sep 2006.

[8] D Hagler and Y Goda. Properties of synchronous and asynchronous release during pulse train depression in cultured hippocampal neurons. *J Neurophysiol*, 85(6):2324–34, Jun 2001.

[9] Y Humeau, F Doussau, N J Grant, and B Poulain. How botulinum and tetanus neurotoxins block neurotransmitter release. *Biochimie*, 82(5):427–46, May 2000.

[10] Jain, V, Murray, JF, Roth, F, Turaga, S, Zhigulin, V, Briggman, KL, Helmstaedter, MN, Denk, W, Seung, and HS. Supervised learning of image restoration with convolutional networks. *Computer Vision, 2007. ICCV 2007. IEEE 11th International Conference on*, pages 1–8, 2007.

[11] M Jiang, L Deng, and G Chen. High ca(2+)-phosphate transfection efficiency enables single neuron gene analysis. *Gene Ther*, 11(17):1303–11, Sep 2004.

[12] R M Kelly and P L Strick. Rabies as a transneuronal tracer of circuits in the central nervous system. *Journal of neuroscience methods*, 103(1):63–71, Nov 2000.

[13] Sergei A Kirov, C Alex Goddard, and Kristen M Harris. Age-dependence in the homeostatic upregulation of hippocampal dendritic spine number during blocked synaptic transmission. *Neuropharmacology*, 47(5):640–8, Oct 2004.

[14] H G Kuypers and G Ugolini. Viruses as transneuronal tracers. *Trends in neurosciences*, 13(2):71–5, Feb 1990.

[15] M Lafon. Rabies virus receptors. *Journal of NeuroVirology*, Jan 2005.

[16] P Lewis and T L Lentz. Rabies virus entry into cultured rat hippocampal neurons. *J Neurocytol*, 27(8):559–73, Aug 1998.

[17] Takahiko Matsuda and Constance L Cepko. Electroporation and rna interference in the rodent retina in vivo and in vitro. *Proc Natl Acad Sci USA*, 101(1):16–22, Jan 2004.

[18] Shakti Narayan, Richard J O Barnard, and John A T Young. Two retroviral entry pathways distinguished by lipid raft association of the viral receptor and differences in viral infectivity. *J Virol*, 77(3):1977–83, Feb 2003.

[19] A Jamila Newton, Tom Kirchhausen, and Venkatesh N Murthy. Inhibition of dynamin completely blocks compensatory synaptic vesicle endocytosis. *Proc Natl Acad Sci USA*, 103(47):17955–60, Nov 2006.

[20] R J O'Brien, S Kamboj, M D Ehlers, K R Rosen, G D Fischbach, and R L Huganir. Activity-dependent modulation of synaptic ampa receptor accumulation. *Neuron*, 21(5):1067–78, Nov 1998.

[21] G Schiavo, M Matteoli, and C Montecucco. Neurotoxins affecting neuroexocytosis. *Physiol Rev*, 80(2):717–66, Apr 2000.

[22] Oksana M Subach, Illia S Gundorov, Masami Yoshimura, Fedor V Subach, Jinghang Zhang, David Grüenwald, Ekaterina A Souslova, Dmitriy M Chudakov, and Vladislav V Verkhusha. Conversion of red fluorescent protein into a bright blue probe. *Chem Biol*, 15(10):1116–24, Oct 2008.

[23] Andrea L Szymczak, Creg J Workman, Yao Wang, Kate M Vignali, Smaroula Dilioglou, Elio F Vanin, and Dario A A Vignali. Correction of multi-gene deficiency in vivo using a single 'self-cleaving' 2a peptide-based retroviral vector. *Nat Biotechnol*, 22(5):589–94, May 2004.

[24] Y Tang, O Rampin, F Giuliano, and G Ugolini. Spinal and brain circuits to motoneurons of the bulbospongiosus muscle: retrograde transneuronal tracing with rabies virus. *J Comp Neurol*, 414(2):167–92, Nov 1999.

[25] G G Turrigiano, K R Leslie, N S Desai, L C Rutherford, and S B Nelson. Activity-dependent scaling of quantal amplitude in neocortical neurons. *Nature*, 391(6670):892–6, Feb 1998.

[26] Gina G Turrigiano. The self-tuning neuron: synaptic scaling of excitatory synapses. *Cell*, 135(3):422–35, Oct 2008.

[27] G Ugolini. Specificity of rabies virus as a transneuronal tracer of motor networks: transfer from hypoglossal motoneurons to connected second-order and higher order central nervous system cell groups. *J Comp Neurol*, 356(3):457–80, Jun 1995.

[28] G Ugolini. Use of rabies virus as a transneuronal tracer of neuronal connections: implications for the understanding of rabies pathogenesis. *Developments in biologicals*, 131:493–506, Jan 2008.

[29] Gabriella Ugolini. Advances in viral transneuronal tracing. *Journal of neuroscience methods*, Jan 2010.

[30] Claudia Verderio, Davide Pozzi, Elena Pravettoni, Francesca Inverardi, Ursula Schenk, Silvia Coco, Véronique Proux-Gillardeaux, Thierry Galli, Ornella Rossetto, Carolina Frassoni, and Michela Matteoli. Snap-25 modulation of calcium dynamics underlies differences in gabaergic and glutamatergic responsiveness to depolarization. *Neuron*, 41(4):599–610, Feb 2004.

[31] Ian R Wickersham, Stefan Finke, Karl-Klaus Conzelmann, and Edward M Callaway. Retrograde neuronal tracing with a deletion-mutant rabies virus. *Nat Meth*, 4(1):47–9, Jan 2007.

[32] Ian R Wickersham, David C Lyon, Richard J. O Barnard, Takuma Mori, Stefan Finke, Karl-Klaus Conzelmann, John A. T Young, and Edward M Callaway. Monosynaptic restriction of transsynaptic tracing from single, genetically targeted neurons. *Neuron*, 53(5):639–647, Jan 2007.

[33] Ian R Wickersham, Heather A Sullivan, and H Sebastian Seung. Production of glycoprotein-deleted rabies viruses for monosynaptic tracing and high-level gene expression in neurons. *Nat Protoc*, 5(3):595–606, Jan 2010.

[34] Corette J Wierenga, Michael F Walsh, and Gina G Turrigiano. Temporal regulation of the expression locus of homeostatic plasticity. *Journal of neurophysiology*, 96(4):2127–33, Oct 2006.

Chapter 5

Concluding Remarks

In summary, we began these studies with the intent to find monosynaptic connections in culture to test computational rules of connectivity. We found that there were limitations to the standard method of patch clamping neurons to find connected pairs. Quite fortuitously, the advances in molecular biology over the past decade have produced several new technologies which promise to make dream experiments possible.

Bibliography

[1] S Bao, VT Chan, and MM Merzenich. Cortical remodelling induced by activity of ventral tegmental dopamine neurons. *Nature*, 412(6842):79–83, 2001.

[2] T V Bliss and G L Collingridge. A synaptic model of memory: long-term potentiation in the hippocampus. *Nature*, 361(6407):31–9, Jan 1993.

[3] E Boyden, F Zhang, E Bamberg, G Nagel, and K Deisseroth. Millisecond-timescale, genetically targeted optical control of neural activity. *Nat Neurosci*, 8(9):1263–8, Sep 2005.

[4] Rodney J Douglas and Kevan A. C Martin. Mapping the matrix: The ways of neocortex, Jan 2007.

[5] Y.Y. Huang and E.R. Kandel. D1/d5 receptor agonists induce a protein synthesis-dependent late potentiation in the ca1 region of the hippocampus. *Proc Natl Acad Sci U S A*, 92(7):2446–50, 1995.

[6] D.H. Hubel and T. N. Wiesel. Receptive fields of single neurones in the cat's striate cortex. *J Physiol (Lond)*, 148:574–91, Oct 1959.

[7] Robert C Malenka and Mark F Bear. Ltp and ltd: an embarrassment of riches. *Neuron*, 44(1):5–21, Sep 2004.

[8] J Olds and P Milner. Positive reinforcement produced by electrical stimulation of septal area and other regions of rat brain. *J Comp Physiol Psychol*, 47(6):419–27, Dec 1954.

[9] NA Otmakhova and JE Lisman. D1/d5 dopamine receptor activation increases the magnitude of early long-term potentiation at ca1 hippocampal synapses. *J Neurosci*, 16(23):7478–86, 1996.

[10] W Schultz. Dopamine neurons and their role in reward mechanisms. *Curr Opin Neurobiol*, 7(2):191–7, Apr 1997.

[11] H Sebastian Seung. Learning in spiking neural networks by reinforcement of stochastic synaptic transmission. *Neuron*, 40(6):1063–73, Dec 2003.

[12] Y Tang, O Rampin, F Giuliano, and G Ugolini. Spinal and brain circuits to motoneurons of the bulbospongiosus muscle: retrograde transneuronal tracing with rabies virus. *J Comp Neurol*, 414(2):167–92, Nov 1999.

[13] Anne M Taylor, Daniela C Dieterich, Hiroshi T Ito, Sally A Kim, and Erin M Schuman. Microfluidic local perfusion chambers for the visualization and manipulation of synapses. *Neuron*, 66(1):57–68, Apr 2010.

[14] Gina G Turrigiano. The self-tuning neuron: synaptic scaling of excitatory synapses. *Cell*, 135(3):422–35, Oct 2008.

[15] G Ugolini. Specificity of rabies virus as a transneuronal tracer of motor networks: transfer from hypoglossal motoneurons to connected second-order and higher order central nervous system cell groups. *J Comp Neurol*, 356(3):457–80, Jun 1995.

[16] G Ugolini. Use of rabies virus as a transneuronal tracer of neuronal connections: implications for the understanding of rabies pathogenesis. *Developments in biologicals*, 131:493–506, Jan 2008.

[17] Ian R Wickersham, David C Lyon, Richard J. O Barnard, Takuma Mori, Stefan Finke, Karl-Klaus Conzelmann, John A. T Young, and Edward M Callaway. Monosynaptic restriction of transsynaptic tracing from single, genetically targeted neurons. *Neuron*, 53(5):639–647, Jan 2007.

[18] Santiago Ramón y Cajal. Comparative study of the sensory areas of the human cortex. page 72, Jan 1899.